NASA CONTRACTOR REPORT

NASA CR-1952

ANALYTIC EVALUATION OF DISPLAY REQUIREMENTS FOR APPROACH TO LANDING

by David L. Kleinman and Sheldon Baron

Prepared by
BOLT BERANEK AND NEWMAN, INC.
Cambridge, Mass. 02138
for Ames Research Center

NATIONAL AERONAUTICS AND SPACE ADMINISTRATION • WASHINGTON, D. C. • NOVEMBER 1971

1. Report No.	2. Government Accession No.	3. Recipient's Catalog No.
NASA CR-1952		

4. Title and Subtitle	5. Report Date
Analytic Evaluation of Display Requirements for Approach to Landing	November 1971
	6. Performing Organization Code

7. Author(s)	8. Performing Organization Report No.
David L. Kleinman and Sheldon Baron	
	10. Work Unit No.

9. Performing Organization Name and Address	11. Contract or Grant No.
Bolt Beranek and Newman Inc. 50 Moulton Street Cambridge, Massachusetts 02138	NAS 2-5962
	13. Type of Report and Period Covered
12. Sponsoring Agency Name and Address	Contractor Report
National Aeronautics and Space Administration Washington, D. C. 20546	14. Sponsoring Agency Code

15. Supplementary Notes

16. Abstract

A computerized analysis procedure, based on a control theoretic model of the human pilot, is used to evaluate display requirements for longitudinal control in the landing approach. The display analyzed employed a digitally generated, perspective runway image with a superimposed artificial horizon for pitch indication. This display is being studied in an experimental program at Ames Research Center. System performance measures are obtained for the approach phase of a light aircraft and a DC-8; predictions are made as to the effects of several display modifications. It is found that augmenting the basic display with glide slope reference bars and a velocity aim point yields adequate performance in calm air. Under moderate turbulence, the augmented display appears to be adequate for a DC-8 approach but not for a light aircraft. Model results are compared with data obtained in Ames' experimental program. The comparison affirms the validity of the pilot model and demonstrates its utility as a display evaluation tool.

17. Key Words (Suggested by Author(s))	18. Distribution Statement
pilot model display evaluation manual control approach to landing optimal control	UNCLASSIFIED-UNLIMITED

19. Security Classif. (of this report)	20. Security Classif. (of this page)	21. No. of Pages	22. Price*
UNCLASSIFIED	UNCLASSIFIED	100	$3.00

*For sale by the National Technical Information Service, Springfield, Virginia 22151

ABSTRACT

A computerized analysis procedure, based on a control theoretic model of the human pilot, is used to evaluate display requirements for longitudinal control in the landing approach.

The display analyzed employed a digitally generated, perspective runway image with a superimposed artificial horizon for pitch indication. This display is being studied in an experimental program at Ames Research Center. System performance measures are obtained for the approach phase of a light aircraft and a DC-8; predictions are made as to the effects of several display modifications. It is found that augmenting the basic display with glide slope reference bars and a velocity aim point yields adequate performance in calm air. Under moderate turbulence, the augmented display appears to be adequate for a DC-8 approach but not for a light aircraft.

In order to adequately reflect the nature of the approach task, the optimal-control model of the pilot was extended to include time-varying effects and visual/indifference thresholds. Model results are compared with data obtained in Ames' experimental program. The comparison affirms the validity of the pilot model and demonstrates its utility as a display evaluation tool.

TABLE OF CONTENTS

LIST OF ILLUSTRATIONS

LIST OF TABLES

INTRODUCTION

The desire for a safe and reliable landing capability under adverse weather conditions has persisted throughout the growth of aviation. If this desire is to become a reality, suitable displays that facilitate pilot performance must be developed. The fundamental questions that arise in the development of such displays concern the information requirements of the pilot: What information should be presented, how, and to what degree of accuracy? In this report, we apply a manned-vehicle system model to obtain answers to some of these questions with respect to a proposed approach and landing display.

The display of interest has as its basic element a digitally generated, perspective runway image, to which is added a horizon bar and airplane symbol. This display could be presented on a cathode ray tube, using information provided by an airborne microwave receiver that senses the location of markers positioned at appropriate points on the airport terrain. It would have application in a low-cost IFR approach system for small airports or as an independently derived, visual back up for automatic landing systems.

Wempe and Palmer [1,2] investigated such a pictorial display in a series of simulator experiments conducted at Ames Research Center (ARC). They found that the display was inadequate with respect to judgement of glide slope errors and control of height. On the other hand, the display had good pilot acceptance, and performance was surprisingly immune to large variations in display resolution and display update rate. It appeared that the deficiencies in the basic pictorial display could be overcome through the addition of appropriate guidance symbology. Consequently,

further experiments were initiated at ARC to examine this possibility. At the same time, the work described herein was undertaken to investigate analytically the potential improvements to the display and to provide a theoretical basis for interpreting the results of the initial and follow-on ARC experiments.

Our analytical study of the display is limited to its use for longitudinal control in approach to landing. Controlling the flight path, by elevator alone, of a light aircraft is the task considered.† The approach starts 10,000 ft. from the runway threshold on a (nominal) 3° glide slope and terminates 1000 ft. from the threshold (at an altitude of about 100 ft.). Power and trim are assumed set to maintain the aircraft on the proper path in the absence of disturbances or spurious pilot inputs. However, a constant vertical draft, sustained for the first 5000 ft. of the approach, disturbs the aircraft from the desired path. In addition, the aircraft is sometimes subjected to random gusts. The choices for the vehicle, nominal flight path and disturbance inputs were dictated largely by the aforementioned ARC experiments.

The central element in our analytic approach to display evaluation is a model of the human pilot that describes his sensing, information processing and control behavior. This model has been documented extensively elsewhere [3,4]. Here, we mention some underlying aspects of the model to provide a point of departure and a proper perspective for this investigation.

---

†It was hoped that this task would minimize the effects of vehicle dynamics and differences in piloting technique on performance with the display [1].

Our model for the human controller blends human response theory within a modern control framework. Its underlying postulate is that the well-trained human controller behaves optimally subject to his inherent limitations and the control task. The major consequence of this hypothesis is that the model contains elements that optimally compensate for the human's limitations. These compensating elements along with our methods of representing pilot limitations are the unique features of the model.

The descriptions of the compensating elements and, in some instances, of the human limitations, have been inspired by modern control theory. In particular, we rely on state-variable methods and models to provide insights for our approach as well as the requisite computational techniques.

In all prior applications of our model, the systems studied were linear and time-invariant. In addition, input disturbances could be modelled as zero-mean, stationary Gaussian noise processes. For such situations, it is relevant and convenient to consider the frequency domain representation of the model. In this context, the model assumes a quasilinear form; it can be used to predict pilot describing functions and power density and remnant spectra. We have found the model capable of predicting these detailed measures of human performance with remarkable fidelity [Refs. 3,4].

In applying our model to approach to landing, we are, however, confronted with an essentially time-varying problem. This is primarily the result of the time-dependent relationship between angular and linear vertical deviations from the glide slope. For example, if the relative error in observing angular deviations from the glide slope is constant, then better estimates of altitude error become available as range decreases. As a result

the quality of the pilots information base improves with time so our model of the human controller is no longer time-invariant. We shall see later that the predictions afforded by this time-varying model are quite remarkable.† The relative ease in extending the model to a time-varying situation is not too surprising in light of its state variable (i.e., time domain) foundations; of course, this was one reason for choosing such a modelling framework.

The experimental conditions that were investigated and the specific display that was employed also necessitated some extensions to the model. In the former case, the use of constant but unknown updrafts was a departure from previous applications in which all inputs were random. Here, too, modern control ideas provided the basis for the solution: the constant wind was considered a "state" to be estimated and was compensated for, in equilibrium, by an optimal, constant "trim" input. In the latter instance, we felt it necessary to include threshold effects in the model to account for experimental judgement data showing large thresholds in the perception of displacements from the glide slope.

Once the necessary extensions to the model had been accomplished, it was a relatively straightforward matter to compute closed-loop performance as a function of various aspects of the display. By and large, our studies paralleled the experimental effort. Thus, we examined the effects of adding guidance symbology, and of changing display resolution, update rate and gain. Results were obtained for both no-turbulence and turbulence conditions. Finally, we computed expected performance with the display in a DC-8 approach task.

---

†We believe that they can be improved even further by a more explicit treatment of true variations in human control strategy (see Chapter 3).

The organization of the report is as follows. The theoretical basis for our display evaluation method is described in Chapter 2. In Chapter 3, the details of applying the method to the problem outlined above are presented. Results of the display analysis are discussed and compared with available experimental data. Concluding remarks are presented in Chapter 4. The mathematical details involved in extending the model are given in the appendices.

THE PILOT-VEHICLE MODEL

A thorough understanding of three fundamental aspects of a manned-vehicle system is essential to achieving the ultimate goal of effective display evaluation. The three basic aspects are: (i) the vehicle dynamics and control task; (ii) the man-machine interaction; and, (iii) the information content and presentation quality of the display. Here we present the theoretical basis of our method for evaluating aircraft displays for use during the final approach to landing.

Vehicle Dynamics and Control Task

The control task that we consider is the piloted approach to landing phase of aircraft flight. In particular, we focus on the portion of the flight from glide-slope insertion to the minimum decision height. As discussed earlier, we analyze the longitudinal control task only, i.e., keeping the aircraft on a nominal glide slope while maintaining proper sink rate in the presence of external disturbances. For these tasks only an elevator is available with which to control the aircraft. Power and trim are set at values that provide a nominal sink rate in the absence of external disturbances.

The vehicle's longitudinal equations of motion (linearized about the nominal glide-path) are given by

$$\begin{aligned}
\dot{u} &= X_u\, u + X_w\, w - g\, \theta \\
\dot{w} &= Z_u\, u + Z_w\, w + U_o\, q + Z_\delta\, \delta - Z_{\dot{w}}\, \dot{w}_g \\
\dot{q} &= M_u\, u + M_w\, w + M_q\, q + M_\delta\, \delta - M_{\dot{w}}\, \dot{w}_g \\
\dot{h} &= -w - u \sin \alpha_o + U_o\, \theta + D(t)
\end{aligned} \tag{1}$$

where

u	perturbed forward velocity (ft/sec)
w	perturbed downward velocity (ft/sec)
θ	pitch angle (degrees)
q	pitch rate (degrees/sec)
h	altitude deviation from glide slope (ft.)
δ	elevator control deflection (degrees)
X_u	$\frac{1}{m}\frac{\partial X}{\partial u}$, drag damping (sec^{-1})
X_w	$\frac{1}{m}\frac{\partial X}{\partial w}$, drag due to angle of attack (sec^{-1})
Z_u	$\frac{1}{m}\frac{\partial Z}{\partial u}$, lift due to velocity (sec^{-1})
Z_w	$\frac{1}{m}\frac{\partial Z}{\partial w}$, vertical damping (sec^{-1})
Z_δ	$\frac{1}{m}\frac{\partial Z}{\partial \delta}$, height control sensitivity ($ft\text{-}sec^{-1}$/degree)
M_u	$\frac{1}{I_{yy}}\frac{\partial M}{\partial u}$, speed stability (degrees/ft-sec)
M_w	$\frac{1}{I_{yy}}\frac{\partial M}{\partial w}$, angle of attack stability (degrees/ft-sec)
M_q	$\frac{1}{I_{yy}}\frac{\partial M}{\partial q}$, pitch damping (sec^{-1})
M_δ	$\frac{1}{I_{yy}}\frac{\partial M}{\partial \delta}$, control sensitivity (sec^{-2})
g	gravitational constant (ft/sec^2)

In Eq.(1), w_g represents random wind turbulence, which we assume is a first-order process. Thus

$$\dot{w}_g(t) = \omega_g\, w_g(t) + \xi(t) \tag{2}$$

where $\xi(t)$ is white-noise with autocovariance

$$E\{\xi(t)\xi(\sigma)\} = \Xi \cdot \delta(t-\sigma) \tag{3}$$

D(t) represents deterministic upwinds. In our analysis, we assume that D(t) is a constant,† $\bar{D}$, whose value is unknown a priori to the pilot. α_o is the nominal glide-path angle and U_o is the nominal steady-state forward velocity, thus $\dot{h}_o = -U_o \sin \alpha_o$ is the nominal sink rate. Equations (1)-(2) may be written more compactly in the state-variable form

$$\dot{\underline{x}}(t) = \underline{A}\, \underline{x}(t) + \underline{b}_\delta\, \delta(t) + \underline{b}_\xi\, \xi(t) + \underline{b}_D\, D(t) \tag{4}$$

where

$$\underline{x} = (w_g,\ u,\ w,\ q,\ \theta,\ h)$$

$$\underline{A} = \begin{bmatrix} -\omega_g & 0 & 0 & 0 & 0 & 0 \\ 0 & X_u & X_w & 0 & -g & 0 \\ -Z_w & Z_u & Z_w & U_o & 0 & 0 \\ -M_w & M_u & M_w & M_q & 0 & 0 \\ 0 & 0 & 0 & 1 & 0 & 0 \\ 0 & -\alpha_o & -1 & 0 & U_o & 0 \end{bmatrix};\ \underline{b}_\delta = \begin{bmatrix} 0 \\ 0 \\ Z_\delta \\ M_\delta \\ 0 \\ 0 \end{bmatrix};\ \underline{b}_\xi = \begin{bmatrix} 1 \\ 0 \\ 0 \\ 0 \\ 0 \\ 0 \end{bmatrix};\ b_D = \begin{bmatrix} 0 \\ 0 \\ 0 \\ 0 \\ 0 \\ 1 \end{bmatrix} \tag{5}$$

†Other representations of D(t) are possible, e.g., winds that decrease linearly with altitude.

The pilot's control task is to fly the aircraft from some initial range R_o (altitude $h_o = R_o \tan \alpha_o$) to an altitude of 100' while minimizing angular deviations from the nominal glide path trajectory.† These angular deviations are given by

$$\alpha(t) \simeq \frac{57.3\, h(t)}{R(t)} . \qquad (6)$$

Thus, we assume that the control task is adequately reflected in the choice of a "commanded" control $\delta_c(t)$ that minimizes the quadratic cost criterion (T_d = time to reach 1000 ft. from the threshold):

$$J(\delta_c) = E\left\{\frac{1}{T_d}\int_0^{T_d}\left[(m_\alpha\,\alpha)^2 + (m_q\,q)^2 + (m_{\dot\delta_c}\,\dot\delta_c)^2\right] dt\right\} \qquad (7)$$

The first term in Eq.(7) is a constant weighting on glide-path errors, the second term is a weighting on pitch rate. It should be noted, for example, that pilots generally do not make rapid pitch motions, a fact which we express mathematically by incorporating a (subjective) weighting on q.††

The weighting on "commanded" control rate, $\dot\delta_c$, is central to our analytic technique. This term may represent an objective or a subjective weighting on a pilot's rate of control. Alternatively, this term could be used to account indirectly for the physiological

†At altitudes below 100' the nature of the control problem is different. From 100' to touchdown (the landing phase) the pilot flares the aircraft, and no longer follows the glide path.

††In our earlier studies of VTOL hovering tasks [3-4] a pitch-rate weighting was also included in the performance functional.

limitations on the rate at which a human can effect control action. We shall have more to say on this point shortly.

Thus, the cost functional weightings m_α, m_q and $m_{\dot{\delta}_c}$ are model parameters that quantify the human's control desires and habits, as well as the requirements of the control task.

It is assumed that the human generates the control $\delta_c(t)$ on the basis of information obtained from viewing a display. (We do not consider kinesthetic cues.) The displayed variables $\underline{y}(t) = [y_1(t),\ldots,y_r(t)]$ may be presented either explicitly (e.g., via meter or indicator) or implicitly (e.g., pictorially). It is assumed that the components of $\underline{y}(t)$ are linear combinations of system states. Thus

$$\underline{y}(t) = \underline{C}(t)\underline{x}(t) + \underline{c}_\delta(t)\delta(t) + \underline{c}_D(t)D(t) \qquad (8)$$

where $\underline{C}(t)$ can be time-varying to model situations in which (gains on) displayed quantities vary with time. The elements of the matrix $\underline{C}(t)$ are determined by a display analysis in cases of implicit presentation.

Pilot Limitations

Any reasonable mathematical model of the pilot-vehicle system must include within its framework the various psycho-physical limitations inherent in the pilot. In this section we discuss the limitations that are incorporated within our analysis.

Time Delay.— The various internal time-delays associated with visual, central processing and neuro-motor pathways are combined and conveniently represented by a lumped equivalent perceptual time-delay, τ.

Neuro-Motor Dynamics.— We do not include "neuro-motor" dynamics directly among the inherent limitations of the human. Recall, however, that we have included in the cost functional (7) a term that depends on control rate. It can be shown [5] that the inclusion of this term results in a first-order lag, $(\tau_N s+1)^{-1}$, being introduced in the feedback controller. Thus, the control rate weighting $m_{\dot{\delta}_c}$ could be used to account for the lag often attributed to the neuro-motor system.

Remnant.— We assume that the various sources of inherent human randomness are manifested as errors in observing displayed outputs and in executing intended control movements. Thus, observation noise, $\underline{v}_y$, and motor noise, δ_m, are our lumped representations of "remnant". These noises represent the combined effects of random perturbations in human response characteristics, time variations in response parameters, and random errors in observing displayed outputs and in generating control inputs.

Thus, the "pilot" is assumed to perceive

$$\underline{y}_p(t) = \underline{y}(t-\tau) + \underline{v}_y(t-\tau) \tag{9}$$

a delayed, noisy replica of the displayed quantities. A single noise $v_{yi}(t)$ is associated with each output $y_i(t)$. Based on studies of controller remnant [6], the noises $v_{yi}(t)$ are assumed to be independent white-noise processes with autocovariances

$$E\left\{v_{yi}(t)v_{yi}(\sigma)\right\} = V_{yi}(t)\cdot\delta(t-\sigma) \quad , \; i=1,2,\ldots,r$$

or (10)

$$E\left\{\underline{v}_y(t)\underline{v}_y'(\sigma)\right\} = \underline{V}_y(t)\cdot\delta(t-\sigma)$$

Furthermore, for foveal viewing conditions, each autocovariance has been found to scale linearly with the variance of its associated output [6]. Thus, at any time t,

$$V_{yi}(t) = \rho_i \cdot E\{y_i^2(t)\} = \rho_i \cdot \sigma_{yi}^2(t) \; ; \; i=1,2,\ldots,r^{\dagger} \tag{11}$$

A numerical determination of the observation noise ratios ρ_i will depend, among other things, on the relevant features (e.g., quality, type and form) of the display panel.

The motor noise, $\delta_m(t)$, which represents random errors in executing the intended control movements, or the fact that the pilot does not have perfect knowledge of the system input, δ, is added to $\delta_c(t)$. Thus,

$$\delta(t) = \delta_c(t) + \delta_m(t) \tag{12}$$

$\delta_m(t)$ is assumed to be a (wide-band) first-order random process generated by

$$\tau_N \dot{\delta}_m(t) + \delta_m(t) = v_m(t) \tag{13}$$

where τ_N is the "motor" lag introduced by the control rate weighting. $v_m(t)$ is white-noise with autocovariance value V_m, or noise-ratio ρ_m.

---

†Equation (11) assumes a zero reference is available. Otherwise, the observation noise scales with the distance of $y_i(t)$ from the nearest scale reference.

Threshold Effects.— There are various nonlinear threshold effects associated with human information processing. For example, if the magnitude of a signal is below a certain level, a pilot may not be able to detect changes in it (visual threshold) or may choose not to react to such changes (indifference threshold). We therefore associate with each displayed variable $y_i(t)$ a visual and/or indifference threshold level, a_i. As with the observation noise ratio ρ_i, values of a_i will be determined by analyzing the given display vis à vis the pilot's inherent limitations.

Thus, each perceived output $y_{pi}(t)$ is modified according to

$$y_{pi}(t) = f_i(y_i(t-\tau)) + v_{yi}(t-\tau) \; ; \; i=1,2,\ldots,r \tag{14}$$

where the threshold nonlinearity $f_i(\cdot)$ is given by

$$f_i(x) = \begin{cases} x-a_i & x \geq a_i \\ 0 & -a_i < x < a_i \\ x+a_i & -a_i \geq x \end{cases} \tag{15}$$

and is shown in Fig. D1.

In Appendix D we use methods of statistical linearization to include the thresholds within our optimization framework. We show that the effect of the threshold is to simply replace the variance σ^2_{yi} in Eq.(11) with a "modified" variance

$$\hat{\sigma}^2_{yi} = \sigma^2_{yi} \cdot \hat{f}_i^{-2} \tag{16}$$

where $\hat{f}_i$ is a (nonlinear) function of a_i and the (mean and) variance of y_i. (See Eq. D12)

The Optimal Control Solution

Our basic assumption in the analysis of pilot-vehicle systems is that the well-trained, well-motivated pilot behaves in an optimal manner, subject to his inherent limitations. Within a control-theoretic framework, therefore, the pilot's control characteristics are determined by the solution of an optimal linear regulator problem with time-delay and observation noise. Optimization problems of this type have been solved by Kleinman [7]. The extensions of the results of [7] to include time-varying observations and deterministic forcing functions are treated in Appendices B and C.

Figure 1 shows the overall structure of the resulting optimal closed-loop system. The feedback portion that pertains specifically to the pilot is shown within the dashed line. The minimizing control is generated by a linear, albeit time-varying, feedback law. Thus, pilot equalization is modelled by the cascade combination of a Kalman filter, a least mean-squared predictor and a set of time-varying gains. However, there is an analytic drawback to this solution. It is that the feedback gains $\underline{\ell}^*$ must be precomputed and their entire time history stored for later on line computation.[†] This awkwardness is common to optimal linear regulators and arises here for two reasons: (1) the time interval $[0,T_d]$ is finite, and (2) the cost functional weights $\alpha(t)$ which is related to the system <u>state</u> $h(t)$ via the transformation

$$\alpha(t) \simeq \frac{57.3h(t)}{R(t)} \tag{17}$$

[†]The gains over the interval $[0,T_d]$ must be computed in <u>backward</u> time, i.e., starting at $t=T_d$. See Athans and Falb [8].

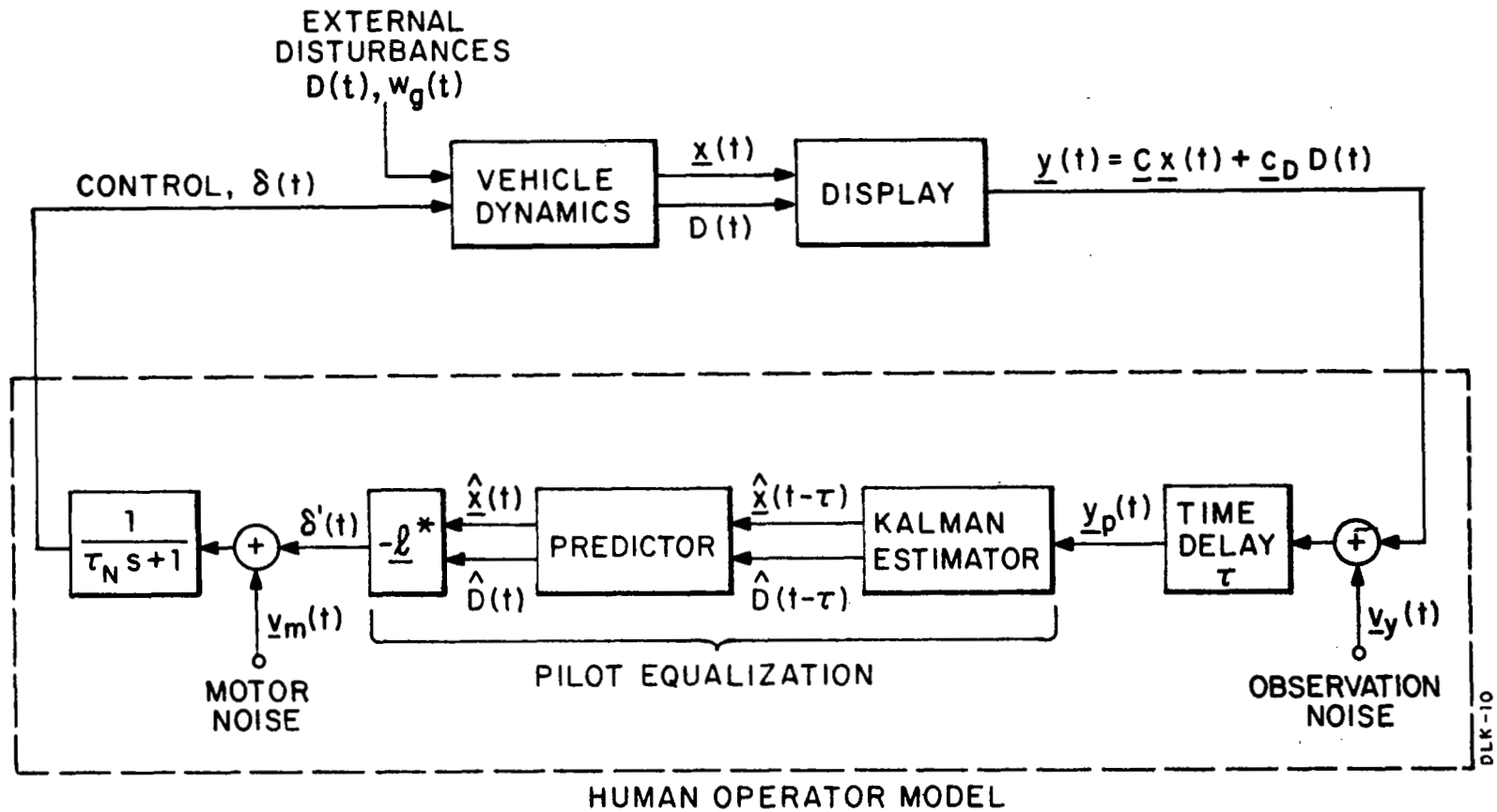

FIG.1 CONTROL THEORETIC MODEL OF OPTIMAL HUMAN BEHAVIOR

Methods for computing "suboptimal" constant or piecewise-constant gains that are more amenable to analytic studies have been developed by Kleinman [9]. Unfortunately, time did not permit our implementation of these techniques. Instead, we computed a single set of constant feedback gains for use over the entire interval $[0,T_d]$. We first let $T_d \to \infty$ in Eq.(7), a reasonable assumption since T_d is generally much greater than system time constants. Second, we replaced the term

$$m_\alpha^2 \, \alpha^2 = \frac{m_\alpha^2}{R^2} \cdot (57.3h)^2$$

in $J(\delta_c)$ with

$$m_h^2 \, h^2 = \frac{(57.3 m_\alpha)^2}{\bar{R}^2} \, h^2 \tag{18}$$

where $\bar{R}$ is an "average" range. We chose $\bar{R} = R_o/2$. The effect of this replacement is obvious: Over the first half of the run the actual penalty on $\alpha(t)$ will be higher than desired, while over the second half the penalty will be smaller than desired. We shall see these effects in later numerical predictions.

With the above modifications, the cost functional (7) becomes

$$J(\delta_c) = \lim_{T\to\infty} \frac{1}{T} E\left\{ \int_0^T [(m_h \, h)^2 + (m_q \, q)^2 + (m_{\dot{\delta}c} \, \dot{\delta}_c)^2] dt \right\} \tag{19}$$

The "commanded" control δ_c that minimizes this expression, conditioned on the perceived information $\underline{y}_p(\cdot)$ in Eq.(9), is given by the linear time-invariant feedback law

$$\tau_N \dot{\delta}_c(t) + \delta_c(t) = -\underline{\ell}^* \hat{\underline{x}}(t) - \ell_D^* \hat{D}(t) \tag{20}$$

Thus, adding Eq.(13) for $\delta_m(t)$ we obtain for the control input δ,

$$\tau_N \dot{\delta}(t) + \delta(t) = -\underline{\ell}^* \hat{\underline{x}}(t) - \ell_D^* \hat{D}(t) + v_m(t)$$

$$\triangleq \delta'(t) + v_m(t) \tag{21}$$

as shown in Fig. 1.

The time-constant τ_N and the optimal gains $\underline{\ell}^*$ and ℓ_D^* are determined via the equations in Appendix A and Ref.[4]. They depend only on the vehicle dynamics and the cost functional weightings. The control rate weighting $m_{\dot{\delta}_c}$ is in 1:1 correspondence with τ_N: the smaller $m_{\dot{\delta}_c}$, the smaller τ_N. This affords a convenient way of adjusting τ_N to a predetermined value.

In the above equations, $\hat{\underline{x}}(t)$ and $\hat{D}(t)$ are, respectively, the model's best estimates of the system state $\underline{x}(t)$ and the value of the constant updraft. These estimates are generated from $\underline{y}_p(\cdot)$ by the Kalman filter and optimal predictor. The Kalman filter yields a best estimate $\hat{\underline{x}}(t-\tau)$, $\hat{D}(t-\tau)$ of the delayed system variables by optimally filtering $y_p(\cdot)$, thus compensating for the observation noise $\underline{v}_y(t)$.† The predictor compensates optimally for the inherent

†The Kalman filter is time-varying since the observation noises in Eq.(9) depend on the signal levels of the displayed outputs as given in Eq.(11).

delay τ by operating on the filter output to generate the estimates $\hat{\underline{x}}(t)$ and $\hat{\underline{D}}(t)$. The equations that describe these linear dynamic feedback elements are obtained from the results of Appendices B and C by defining an "augmented" state vector $\underline{\chi}(t) = [\underline{x}(t), \delta(t), \underline{D}(t)]$ and combining Eqs.(4) and (21) into a single equation for $\dot{\underline{\chi}}(t)$.

Note that the feedback system generates a best estimate of $\underline{D}(t)$. The estimation, and the compensating control input that gets generated, results in a closed-loop transient. This time-varying adaptability of the model to nonrandom inputs is an important extension to our earlier results (Ref.4).

Model Outputs for Display Evaluation

The structure of Fig. 1, coupled with the equations in Appendices A - D completely determine the optimal closed-loop system. In order to use the optimal control model in a predictive manner as a systems analysis tool, we require the prespecification of various input parameters relating to the vehicle configuration, the task description and the pilots limitations. These inputs are, in summary,

1. The Vehicle Description: the equations of motion and the characteristics of the external disturbances.
2. The Task Description: the cost functional weightings; both objective and subjective.
3. The Display Parameters: which quantities are displayed and to what degree of accuracy.
4. The Pilot Limitations: observational time delay τ, motor lag τ_N, motor noise ratio ρ_m. An observation noise ratio ρ_i and a threshold a_i associated with each displayed quantity. ρ_i and a_i are functions of the particular display vis à vis human factors considerations.

Once the model inputs are specified we may obtain predictions of such useful output quantities as:

1. The mean time history of any state, output or the control. This represents the flight path one would expect to find by averaging the results of many runs.†

2. The variance at any time t of any state, output or control about its computed mean value. This variability arises from the system's random inputs, i.e., gust disturbances,and "remnant".

3. The mean and variance at any time t of the model's estimate of the system state $\underline{x}(t)$. Thus we are able to predict what the pilot thinks the system is doing as well as what the system is actually doing. These predictions are essential to analyzing the decision-making role of the pilot.

4. The model's estimate of the deterministic updraft $\hat{D}(t)$. A time history of $\hat{D}(t)$ will show how rapidly the pilot model can recognize the updraft and compensate accordingly.

5. The probability distribution of any system variable at time t. These distributions are necessary for predicting probability of a successful landing, go-around, etc.

In addition to the above dynamic measures of system response, we may also obtain various static measures. For example, we could consider a tracking task performed at some fixed distance from the runway. In this case, predictions can be made of pilot describing functions as well as various power density spectra.††

†Thus, the mean trajectory can be associated with the system's response to the deterministic input D(t).

††Recall that these quantities have little meaning in the time-varying case.

A computer program, PIMAL (Pilot Model for Approach to Landing) has been written for generating the above predictions. Inputs to the program are the system quantities $\underline{A}$, $\underline{b}_\delta$, $\underline{C}$; the cost functional weightings m_α and m_q; the human response parameters τ, τ_N, ρ_m, the observation noise ratios ρ_i and the threshold limits a_i. The computer program is highly interactive and very easy to use. Any one, or several model input parameters can be changed simultaneously. This enables rapid on-line predictions of the effects of changes in the vehicle, the display or even the human.

Having established the means for system performance predictions, PIMAL can be used in a systematic fashion to analyze an information display and to study the effects of changes in display format. Changes in the nature of the display are reflected as changes in various program inputs. Adding or removing displayed quantities will change the output transformation in Eq.(8). Changes in display resolution, gain, scale markings, etc will require changes in ρ_i and/or a_i. Changes in display update rate may be modelled by changing the equivalent perceptual time-delay τ.

In this manner it becomes relatively straightforward to investigate the effects of display modifications on closed-loop system performance. These predictions, coupled with a sensitivity analysis about a nominal display condition, provide an analytic method for evaluating aircraft displays within the context of a piloted approach to landing task. In the next section the model is used to analyze the pictorial display developed at NASA-ARC for approach to landing. The model predictions are compared with results of simulator experiments performed at Ames and described in Ref.[1,2].

DISPLAY EVALUATION

In this chapter we apply the analytic techniques we have developed to the pilot-vehicle-display system studied by Palmer and Wempe [1,2]. We describe the task and the display and use the model to predict measured performance data across a variety of display configurations. The results we obtain demonstrate the value of our control-theoretic approach for display evaluation.

Vehicle Dynamics and Display Configuration

The dynamics of a Navion, a low-wing four passenger light aircraft,were simulated in the experiments. The longitudinal equations of motion are given by Eq.(1); numerical values for the stability derivatives are:

$X_u = -.045\ \text{sec}^{-1}$ $\quad M_u = 0$

$X_w = .036\ \text{sec}^{-1}$ $\quad M_w = -2.86\ \text{deg/ft-sec}$

$Z_u = -.3697\ \text{sec}^{-1}$ $\quad M_q = -2.077\ \text{sec}^{-1}$

$Z_w = -2.024\ \text{sec}^{-1}$ $\quad M_\delta = -11.19\ \text{sec}^{-2}$

$Z_\delta = -.491\ \text{ft-sec}^{-2}/\text{deg}$ $\quad U_o = 176./57.3 = 3.06\ \text{ft-sec}^{-1}/\text{deg}$

The nominal flight path was a 3^o glide slope that intersected the runway at a point 1000' beyond the threshold. At the beginning of each simulated flight the aircraft was positioned level on the glideslope, 10,000' from the threshold. Thus,

$R_o = 11{,}000$ ft. $\quad \alpha_o = 3^o = .05234$ rad

$h_o = 576$ ft. $\quad \dot{h}_o = 9.2$ ft/sec $= 552$ ft/min

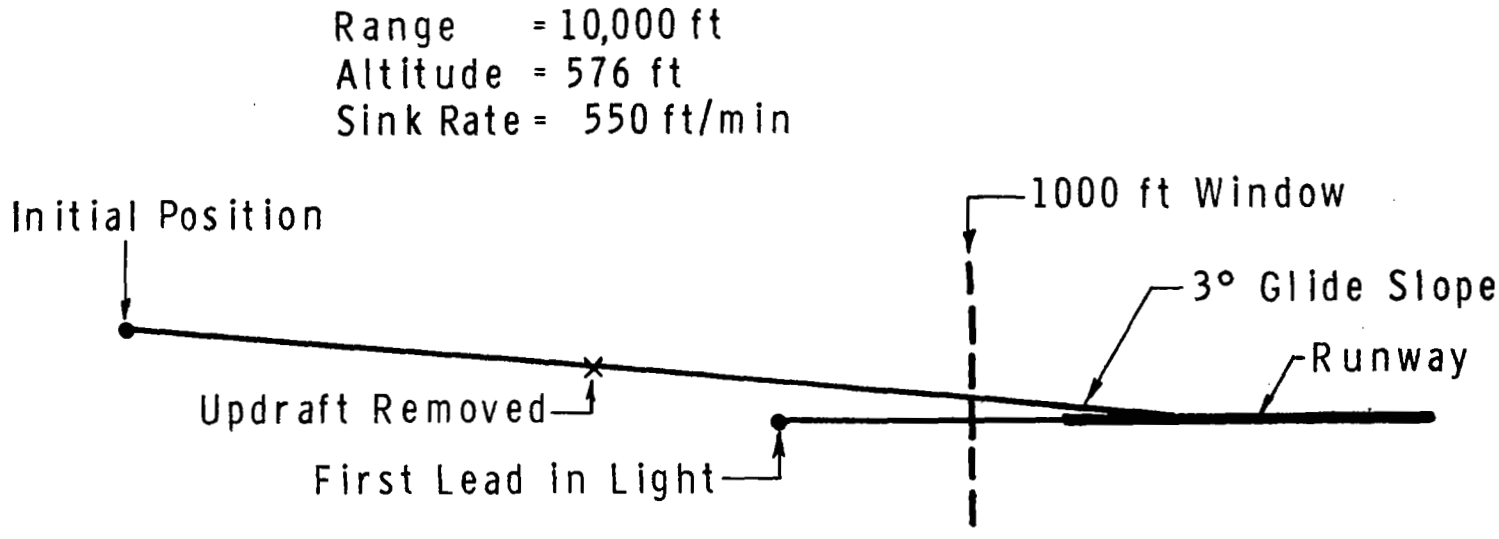

FIG. 2 FLIGHT PATH GEOMETRY

On each of the flights, a constant vertical draft was applied to the aircraft and sustained for the first 5000' of the approach. The value of the draft was selected randomly from the set $\bar{D}$ = {-3.0, -1.5, +1.5, +3.0}. After 5000' the vertical drafts were eliminated.† The pertinent flight path geometry is depicted in Fig. 2.

On one half of the flights moderate turbulence was simulated. The random wind turbulence w_g had a break frequency of ω_g = 0.5 rad and an RMS level σ_{wg} = 3.0 ft/sec.

The display configuration is described in detail in Refs. [1]-[2]. Here we indicate only the salient features of the display pertinent to aircraft longitudinal control during the approach phase.†† We consider that portion of the flight from 10,000 ft. to 1000 ft. from the runway threshold. Thus, termination of the approach occurs at an altitude of about 100 ft.

Figure 3 shows the basic display presentation. A runway image, horizon bar and aircraft reference symbol provided a perspective view of the real world. The display was generated on a cathode ray tube by a 946 line TV system. The displayed field of view was 40^{o} by 40^{o} in the real world with a display gain of 1/2 at the pilot's eye. The nominal runway image quality was $.05^{o}$ resolution; the image was updated every 0.1 sec.

---

†In the experiments the wind drafts were reduced exponentially to zero. In our analytic study, however, we assume that the winds are suddenly terminated at 5000 ft. The effects of the "fade-out" difference are not very important since the experimental time constants were small. However, our predicted $\dot{h}$ will experience a step (rather than an exponential) change at 5000 ft.

††Display configurations pertinent to touchdown are not considered herein.

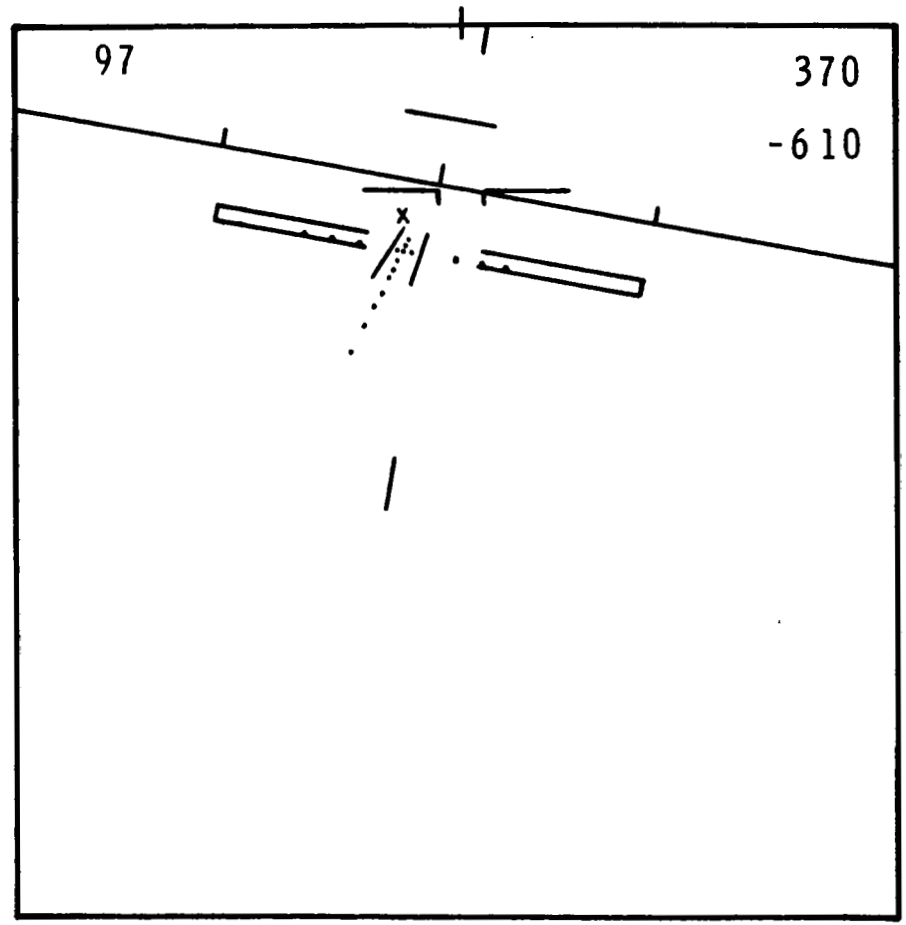

FIG. 3 AUGMENTED PICTORIAL DISPLAY FOR APPROACH TO LANDING SHOWING GLIDE-PATH REFERENCE BARS AND VELOCITY VECTOR SYMBOL X

In addition to the above elements, the display also contained glide slope reference bars which were depressed 3^{o} below the horizon. These bars "augment" the visual cue that says if the glide slope intersection point on the runway is 3^{o} below the true horizon, the aircraft is on a 3^{o} glide slope [2]. The angular separation of the reference bars was $2\beta\alpha_{o}$, i.e., a nominal $\pm\beta\alpha_{o}$ degrees about the glide slope intersection marking. In the experiments β=.1.

In some of the experimental configurations a velocity vector symbol (the X in Fig. 3) was added to the display. The "X" shows the ground point towards which the aircraft's velocity is directed at any instant. Vertically it provides flight path angle information. Thus, the deviation of the X from the glide-slope intersection point is an indication of sink rate deviations $\dot{h}(t)$ or $\dot{\alpha}(t)$.

In summary therefore, the display provides the pilot with observations of glide slope angular deviations $\alpha(t)$ as well as of $\dot{\alpha}(t)$. In addition, the pilot also perceives pitch $\theta(t)$ and pitch rate $q(t)$[†] from the artificial horizon and aircraft symbol. We assume that the pilot can obtain range information, $R(t)$, from the horizontal visual angle subtended by the width of the runway at the glide slope intersection point. This angle is given by

$$\alpha_{r} = k_{d} \cdot \frac{150}{R} \; ; \; k_{d} = \text{display gain} \qquad (22)$$

where 150' is the runway width. Finally, in cases where the velocity vector symbol X is displayed, we assume that the pilot obtains <u>explicit</u> $\dot{h}(t)$ information (as opposed to the implicit $\dot{\alpha}(t)$ information obtained from the glide slope indicator).

[†]We assume that if a quantity is explicitly presented, the pilot also obtains, implicitly, the rate of change of that quantity [6].

Model Parameters

In order to apply the optimal control model to analyze the approach to landing task, we must determine numerical values for the display matrix $\underline{C}(t)$ in Eq.(8). In addition, values are needed for the various human response/display parameters τ, τ_N, ρ_m, ρ_i, a_i, i=1,2,...,r discussed in the preceding chapter. We shall see that parameter values are quite easily chosen a priori by combining human response results with the considerations of the control task and display.

We first relate perception of glide slope deviations $\alpha(t)$ to perception of height deviations h(t). This is convenient because it allows us to treat h(t) as a "displayed output" in our analyses.† The pilot observes $\alpha(t)$ with the aid of the displayed glide slope reference bars. Thus, the observation noise $v_\alpha(t)$ has autocovariance

$$E\{v_\alpha(t)v_\alpha(\sigma)\} = \rho_\alpha \hat{f}_\alpha^{-2} \cdot E\{[\beta\alpha_o - |\alpha(t)|]^2\} \cdot \delta(t-\sigma) \quad (23)$$

where $\hat{f}_\alpha$ is the equivalent gain of the threshold (15) associated with observations of $\alpha(t)$, (see Appendix D). Note that $\beta\alpha_o - |\alpha(t)|$ is the separation between $\alpha(t)$ and the nearest reference bar.

In addition to $\alpha(t)$, the pilot perceives directly range R(t) with observation noise $v_R(t)$ where

$$E\{v_R(t)v_R(\sigma)\} = \rho_R\, E\{[R(t)]^2\} \cdot \delta(t-\sigma) = \rho_R \sigma_R^2(t) \cdot \delta(t-\sigma) \quad (24)$$

---

†Since h(t) is a state variable, the output matrix $\underline{C}(t)$ will be constant. However, the observation noise matrix $\underline{V}(t)$ will be time-varying. Alternatively, if we wished to treat $\alpha(t)$ as the displayed variable, $\underline{V}(t)$ would be constant while C(t) would be time-varying. The two approaches are equivalent since $\underline{C}(t)\underline{V}^{-1}(t)\underline{C}(t)$ is what appears in the equations that define the model and α and h are related by $h=\alpha R$. However, it is more convenient to work with a constant $\underline{C}$.

The observation noise $v_h(t)$ associated with perception of $h(t) = R(t)\alpha(t)$ is obtained from

$$v_h(t) \simeq \alpha(t)v_R(t) + R(t)v_\alpha(t) \tag{25}$$

Combining Eqs.(23)-(25) we see that $v_h(t)$ has autocovariance

$$V_h(t) = \rho_\alpha \hat{f}_\alpha^{-2} \cdot E\{[\beta H_o(t) - |h(t)|]^2\} + \rho_R E\{h^2(t)\} \tag{26}$$

where $H_o(t) = R(t)\alpha_o$ is the altitude of a 3^o glide slope at distance $R(t)$.

The quantity $\dot{\alpha}(t)$ is perceived from observations of $\alpha(t)$. The observation noise $v_{\dot{\alpha}}(t)$ has autocovariance

$$E\{v_{\dot{\alpha}}(t)v_{\dot{\alpha}}(\sigma)\} = \rho_{\dot{\alpha}} \hat{f}_{\dot{\alpha}}^{-2} E\{\dot{\alpha}^2(t)\} \cdot \delta(t-\sigma). \tag{27}$$

However, values of $\sigma_{\dot{\alpha}}^2(t) = E\{\dot{\alpha}^2(t)\}$ for this task are extremely small since $\dot{\alpha} \simeq (\dot{h}-U_o\alpha)/R$. For example, if $\dot{h}$=1 ft/sec at R=5000' then $\dot{\alpha} \simeq .01^o$/sec which is less than human visual thresholds on rate perception. Therefore, we assume that no useful $\dot{\alpha}$(or $\dot{h}$) information is obtained from the glide slope indicator.

Pitch and pitch rate are also displayed outputs. The thresholds associated with these quantities were neglected in the analysis as they were deemed insignificant for the display used. Thus,

$$E\{v_\theta(t)v_\theta(\sigma)\} = \rho_\theta \sigma_\theta^2(t) \cdot \delta(t-\sigma) \tag{28}$$

$$E\{v_q(t)v_q(\sigma)\} = \rho_q \sigma_q^2(t) \cdot \delta(t-\sigma) \tag{29}$$

Finally, in cases where the aim point symbol is displayed, we assume that the pilot obtains explicit sink rate information $\dot{h}(t)$ as discussed earlier. The observation noise $v_{\dot{h}}(t)$ has autocovariance

$$E\{v_{\dot{h}}(t)v_{\dot{h}}(\sigma)\} = \rho_{\dot{h}} E\{\dot{h}^2(t)\} \cdot \delta(t-\sigma) , \tag{30}$$

where we assume a zero threshold on $\dot{h}(t)$ perception.

The perceived outputs $\underline{y}_p(t)$ may be written, combining the preceding equations, in vector form

$$\begin{aligned} \underline{y}_p(t) &= \underline{y}(t-\tau) + \underline{v}_y(t-\tau) \\ &= \underline{C}\ \underline{x}(t-\tau) + \underline{c}_D\ \bar{D} + \underline{v}_y(t-\tau) \end{aligned} \tag{31}$$

where $\underline{y}(t) = \text{col}[h,\dot{h},\theta,q]$, $\underline{v}_y = \text{col}[v_h, v_{\dot{h}}, v_\theta, v_q]$ and

$$\underline{C} = \begin{bmatrix} 0 & 0 & 0 & 0 & 0 & 1 \\ 0 & -\alpha_o & -1 & 0 & U_o & 0 \\ 0 & 0 & 0 & 0 & 1 & 0 \\ 0 & 0 & 0 & 1 & 0 & 0 \end{bmatrix}, \quad \underline{c}_D = \begin{bmatrix} 0 \\ 1 \\ 0 \\ 0 \end{bmatrix}$$

The autocovariances of the observation noises are given by Eqs. (26)-(31). The covariance of $v_{\dot{h}}$ is assumed infinite when the aim point is not displayed.

The equivalent perceptual time-delay τ in Eq.(31) also includes the display update rate of 0.1 sec. When this is added to a nominal human delay of .2 sec, we obtain τ=.3 sec.

The various observation noise ratios $\rho_\alpha, \rho_{\dot{h}}, \rho_\theta, \rho_q, \rho_R$ in Eqs.(26)-(31) were set equal to $.01\pi$ (i.e., -20 dB white noise power density level). This value has been found appropriate to foveal viewing of good resolution displays [6]. The noise ratios being set equal is a reflection of the fact that an integrated display was used so that visual scanning did not appear to be necessary.†

The visual/indifference threshold, a_α, associated with glide path deviations $\alpha(t)$ was taken to be .1 degree. Several reasons prompted this choice: (a) The vertical resolution of the display was $.05^\circ$. With a display gain $k_d = 1/2$ the resolution on α would be $.1^\circ$, (b) A typical value for the human threshold on position quantities is $.05^\circ$ of visual arc (see Appendix D). Since $k_d = 1/2$, we again find $a_\alpha = .1^\circ$, (c) Pilots performing an approach to landing task generally will not try to control $\alpha(t)$ any more precisely than to within $\pm .1^\circ$ of the desired glide slope (i.e., keeping within the center dots on an ILS indicator). This translates to keeping the glide path dots within the middle third of the glide-path reference box (Fig.3).

The cost functional $J(\delta_c)$ for this task is given by Eq.(19). The weighting m_h is related to the constant weighting m_α on glide path deviations according to

$$m_h = \frac{57.3 m_\alpha}{\bar{R}} \simeq .01\, m_\alpha \tag{32}$$

For this task we chose relative weightings $m_\alpha/m_q = 0.5$.

---

†In cases where there are several (nonintegrated) displays, methods for including scanning or attentional constraints within the optimal control framework are developed in Refs. [4,10].

Thus, we balanced a glide path error of 1^{o} with a pitch rate correction of $.5^{o}$/sec. A pitch rate of $.5^{o}$/sec results in a 3 ft/sec change in sink rate after 2 seconds. These numbers seemed reasonable for the given vehicle and control task.† Therefore,

$$m_h = .005, \; m_q = 1.0, \; m_{\dot{\delta}_c} = .14 \tag{33}$$

The weighting $m_{\dot{\delta}_c}$ on control rate was adjusted to yield a time constant $\tau_N = .1$ sec in the feedback loop. This value is typical for the neuromotor time constant and has been found to be appropriate to the model across a wide range of tracking tasks [4].

The final model parameter that must be specified is the motor noise covariance V_m (or motor noise ratio ρ_m). The motor noise $v_m(t)$ is added to $\delta'(t)$ in Eq.(21). Thus we assume, with analogy to the observation noise, that

$$V_m = \rho_m \, E\{[\delta'(t)]^2\} \tag{34}$$

Typical values for ρ_m have been found to be $.003\pi$ - $.01\pi$, i.e., -20 to -25 dB white noise power density level [3 , 4]. In the computer program that was developed we did not include a means for specifying ρ_m directly. Instead, values of V_m were chosen and the resulting noise ratios were then checked for reasonableness. Typically, values of $\rho_m \approx$ -22 dB resulted.

---

†One would expect that any reasonable choice of m_α/m_q should suffice. This is indeed correct, as sensitivity studies using the model have shown. The trade-offs between glide-slope error and control effort do vary somewhat among pilots. The ratio we chose was intended to be representative.

Experimental and Predicted Results

Having prespecified all of the input parameters we now apply the model to analyze the approach to landing task. In particular, we use the computer program PIMAL described in the preceding chapter to predict the (statistical) time histories of pertinent system variables across different display configurations. Comparison is made with the experimental results of Palmer and Wempe. Their data consisted, for each simulated flight, of the integrated mean and RMS of $\theta, q, \dot{h}, \alpha, \delta$. For a particular quantity $x(t)$ the mean and RMS that were measured were

$$\bar{x} = \frac{1}{N} \sum_{i=1}^{N} x(t_i) \quad , \; N = \text{number of samples} \tag{35a}$$

$$\text{RMS} = \sqrt{\frac{1}{N} \sum_{i=1}^{N} x^2(t_i)} \tag{35b}$$

The various measurements were then averaged over several identical runs for reliability.[†]

Measurements of mean and RMS were made over both range intervals

$$\begin{aligned} R_1 &= (10{,}000'\text{-}5000') \\ R_2 &= (5{,}000'\text{-}1000') \end{aligned} \tag{36}$$

[†]In using the equations of Appendix C to predict these experimental results we implicitly assume an ergodic property, namely, that the (ensemble) average of the time integrals is equal to the time integral of the (ensemble) average.

In addition, altitude was recorded at distances from the threshold of 5000' and 1000'.

For simplicity in the analysis, we consider only the case of updrafts of +3 ft/sec, i.e., $\bar{D} = 3$. We shall be concerned with the effects of turbulence, display modifications, display gain, update interval and resolution upon overall closed-loop performance.

Runway Pictorial Display.— The original display that was first considered by Wempe and Palmer [1] contained only a runway image and an artificial horizon. There were neither glide slope reference bars nor an aim point. We analyze this original display to place in perspective the various display features that were subsequently added. We study the no turbulence case only.

In our analysis the threshold associated with perception of $\alpha(t)$ was taken as 0.5°. This value was chosen on the basis of experimental height judgment† data obtained with the given display [1]. (Note that this implies that the visual/indifference threshold is a function of display format.) In addition, since there were no reference bars we set $\beta=1$ in Eq.(26). All other model input parameters were at their nominal, a priori, values.

The model's prediction of aircraft altitude vs. distance from the threshold is shown in Fig. 4. We show the mean response and the variability ($\pm 1\sigma$) that arises from pilot induced randomness (remnant). It is clear from these results that pilots using this display would be unable to control the aircraft to within $\pm .3^{\circ}$ of the nominal glide slope. The reason is simply that the display provided inadequate height information. As a result, the model's estimate of the updraft was in error by 50% at 5000'.

†Judgments made from above glide-slope. Experiments showed that pilots were unable to estimate their position from the glide slope to better than $\pm .5^{\circ}$ using only the runway pictorial image as a cue.

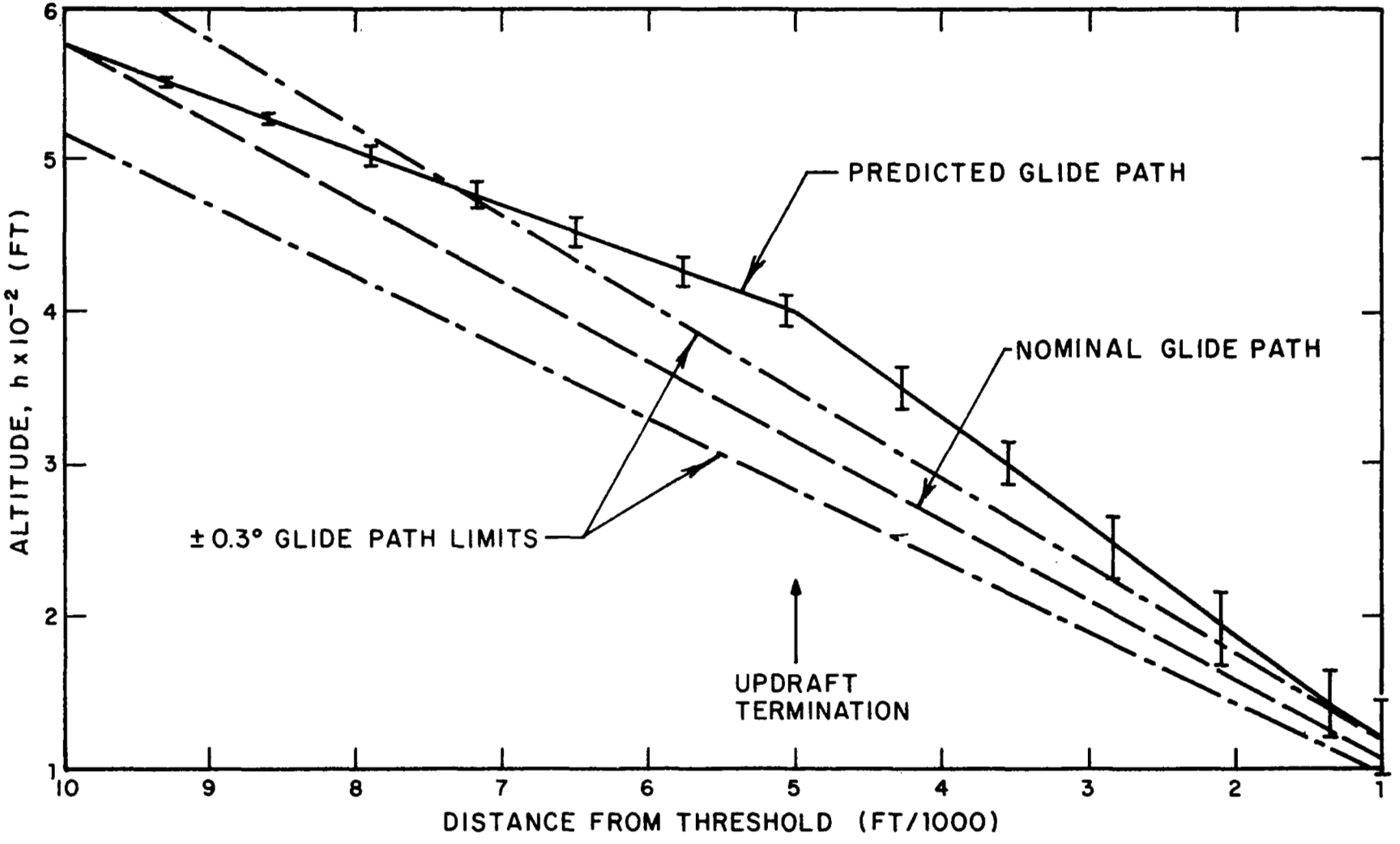

FIG. 4 PREDICTED PERFORMANCE: NO DISPLAY AUGMENTATION, NO TURBULENCE

The aircraft drifted off the glide path by as much as .8 degrees, even though the threshold on α was .5!

The predicted results indicate, that at a distance of 5000' from the runway threshold, the aircraft altitude is 397 $\pm$ 11 ft. If no compensating corrections had been made, the aircraft would have been at h=399 ft. At 1000' from the threshold, predicted altitude is h=119 $\pm$ 21 ft (i.e., average error = 14 $\pm$ 21 ft). These results agree quite well with experimental data [1], which also demonstrated the display's inadequate presentation of height information.

Addition of Glide Slope Reference Bars.—
No Turbulence-- Based primarily on the experimental results, it was decided to modify the above display to include glide slope reference markings at $\alpha=\pm.3^{o}$ [2]. This yields improved $\alpha(t)$ information. The resultant display is as described in the preceding sections and served as a basis for the second experimental program performed at Ames Research Center.

In order to judge the effectiveness of the display modification, the model was used to predict system performance for the same conditions (i.e., updraft = +3 ft/sec, no turbulence) analyzed above. The model parameters are invariant except for the visual/indifference threshold on $\alpha(t)$ which is $.1^{o}$ and the reference ratio β which is .1. These correspond to the particular display configuration used.

The predicted histories of glide slope error, h(t), pitch, $\theta(t)$, and sink rate, $\dot{h}(t)$, are shown in Fig. 5. With this display, the pilot model was capable of controlling average glide slope errors to within $\pm.2^{o}$. However, note that the aircraft travels

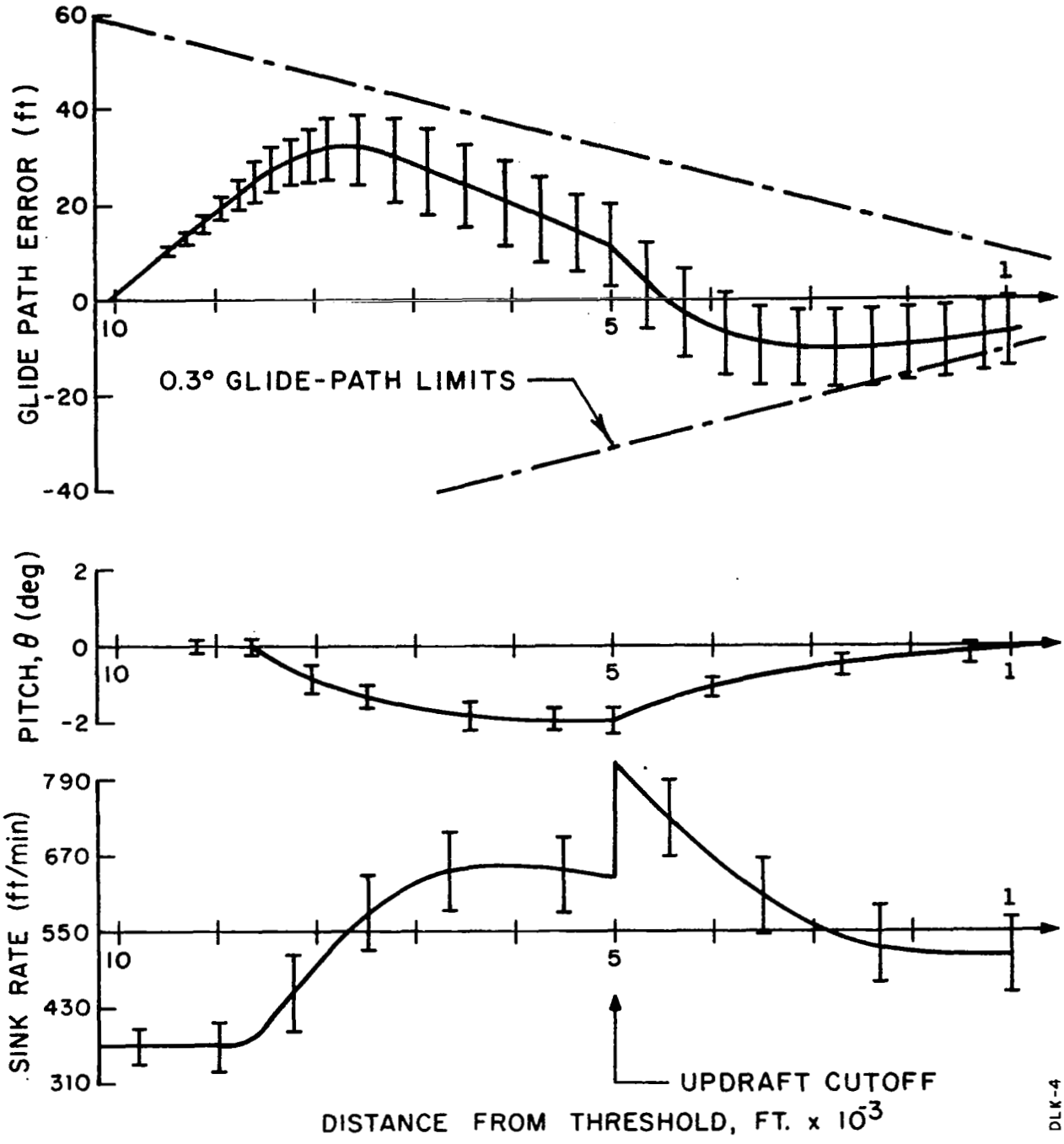

FIG. 5 PREDICTED PERFORMANCE: GLIDE PATH REFERENCE BARS AUGMENTATION, NO TURBULENCE

some 1500' before pilot correction is initiated. This "dead-zone" arises from the initial lack of $\alpha(t)$ information (while $\alpha(t)$ is less than its $.1^{o}$ threshold) coupled with the lack of $\dot{h}(t)$ information. When the updraft is removed, the decent rate quickly increases and the aircraft is seen to undershoot the desired glide path. Changes in aircraft pitch are made smoothly, as a result of the cost functional weighting on $q(t)$. We thus see the model "trim out" the effects of the constant wind by adding a compensating offset in pitch. When the wind is terminated the trim is reduced (slowly) to zero.

Ensemble averages at various points along the state trajectories were not obtained in experiment. Instead, as mentioned earlier, measurements were obtained of the time-averaged mean and RMS as in Eq.(35). A comparison of this data with model predictions is shown in Table 1.† The numbers in parenthesis are the 1-sigma experimental variability. As can be seen, predicted and measured results are in remarkable agreement over both intervals. The fact that the RMS results agree so well is evidence of the validity of our model of the human's limitations. Since there is no turbulence,the system's only randomness arises from the pilot himself. The excellent agreement of mean performance is evidence of the model's ability to predict the time-varying adaptability of the pilot to the presence of the deterministic updraft.

There is only one set of numbers for which model predictions are not within one S.D. of the data. This occurs for mean and RMS α over R_2.

---

†The experimental data is the average over display conditions 1 and 2 described in Ref.[2]. These conditions differed only slightly for the approach phase and we do not make a distinction between them in our analysis.

TABLE 1

MODEL AND MEASURED PERFORMANCE:† REFERENCE BARS, NO TURBULENCE

	Mean (10-5000') RMS				Mean (5-1000') RMS			
	Model	Measured	Model	Measured	Model	Measured	Model	Measured
q(deg/sec)	-.07	-.06(.01)	.31	.29(.09)	.08	.06(.03)	.31	.35(.14)
θ(degrees)	-1.05	-1.0(.10)	1.36	1.24(.18)	-.73	-.89(.2)	.96	1.13(.25)
δ_e(degrees)	.21	.21(.03)	.32	.29(.03)	.49	.50(.03)	.53	.52(.04)
$-\dot{h}$(ft/min)	531.	531(19)	547.	542(24)	602.	621(37)	612.	633(35)
α(degrees)	.15	.13(.03)	.17	.14(.04)	-.12	.04(.05)	.20	.12(.06)
H_T(feet)	325	330	σ=9	σ=8	98	107	σ=8	σ=7

†Measured data is the average of 11 runs.

The discrepancy is understandable if we recall our discussion on the average weighting on h(t) in the cost functional (19). With a fixed weighting m_α on glide slope error $\alpha(t)$, the equivalent weighting on altitude deviations is given by

$$m_h \simeq \frac{57.3\ m_\alpha}{R(t)}$$

and increases inversely with range. Thus, as R(t) decreases m_h must increase, a fact which is not incorporated into the model since we have chosen a constant m_h appropriate to $R = \bar{R} = 11{,}000/2$. The relationship between m_h and distance from threshold is given in the table below for $m_\alpha/m_q = 0.5$.

Distance from Threshold	m_h
10000 - 9000	.0030
9000 - 8000	.0034
8000 - 7000	.0038
7000 - 6000	.0044
6000 - 5000	.0052
5000 - 4000	.0064
4000 - 3000	.0082
3000 - 2000	.011
2000 - 1000	.019

It can be seen that the value $m_h \simeq .005$ that we have chosen is not a good approximation over the entire range, and is relatively poorer for smaller R(t). The obvious way around this difficulty is to solve the optimization problem with a piecewise constant or a time-varying m_h, thereby obtaining feedback gains that change as R(t) decreases. The result of this modification would

be to decrease RMS and mean glide path deviations as range decreases. For example, if over R_2 we were to choose a constant value of $m_h \approx .01$ (corresponding to 2500') we would expect RMS $\alpha(t)$ to be approximately .1 deg as contrasted with .2 deg found earlier and .12 deg found experimentally.†

It therefore appears that the inclusion of piecewise constant gains within the pilot model would further enhance the reliability of the resulting predictions by representing more accurately the truly time-varying nature of the approach task.

Effects of Turbulence-- In order to evaluate the performance of the pilot-vehicle-display system under moderate turbulence conditions, we added random gusts w_g to the vehicle as in Eq.(1). The mean and variance of pertinent system quantities, at various distances from the threshold, were computed in the same manner as before. The resulting mean trajectories were virtually identical to those of Fig. 5, while the variance was somewhat larger because of the turbulence. For this reason the trajectories were not plotted.

A comparison of measured and predicted mean and RMS performance is given in Table 2.†† Once again the agreement is excellent over both intervals, with the possible exception of RMS $\alpha(t)$ over 5-1000'. The predicted mean quantities are virtually identical to those in Table 1; indeed measured means do not differ significantly from the no-turbulence results. Measured and predicted

†Mean glide-path errors over R_2 are influenced to some extent by the fact that the pilot knows the updraft is to terminate at 5000' and can anticipate his control action accordingly. On the other hand, the model is nonanticipative and must wait until the updraft is removed to begin corrective action.

††The measured data is somewhat erratic due to the highly variable nature of the experimental turbulence waveform.

TABLE 2

MODEL AND MEASURED PERFORMANCE:† REFERENCE BARS, TURBULENCE

	Mean (10-5000') RMS				Mean (5-1000') RMS			
	Model	Measured	Model	Measured	Model	Measured	Model	Measured
q(deg/sec)	-.07	-.05(.04)	.81	1.1(.12)	.08	.10(.07)	.81	1.25(.18)
θ(degrees)	-1.05	-.98(.38)	1.69	1.40(.36)	-.71	-.54(.57)	1.44	1.29(.28)
δ_e(degrees)	.21	.20(.08)	.38	.42(.07)	.48	.40(.18)	.58	.59(.14)
$-\dot{h}$(ft/min)	529.	527.(30)	557.	578.(30)	600.	629.(59)	624.	668.(63)
α(degrees)	.14	.17(.12)	.19	.20(.12)	-.09	.02(.12)	.37	.20(.07)
w_g(ft/sec)	0.0	.06(1.16)	3.0	3.12(.32)	0.0	.96(.84)	3.0	3.0(.78)
H_T(feet)	326.	330	σ=20	σ=13	100.	104	σ=20	σ=13

†Measured data is the average of 13 runs.

RMS quantities show increases over the no turbulence case. Notable are the increases in q over both intervals R_1 and R_2 and the 80% increase in RMS α (both measured and predicted) over interval R_2. Standard deviations in the altitudes at 5000' and 1000' also show large increases over the no turbulence case. Note that RMS control over R_2 shows only a small increase attributable to turbulence. These results again demonstrate that mean response is associated with deterministic signals, whereas response variability is associated with pilot remnant and external randomness.

We see that the addition of the reference bars is a significant improvement to the display and to the resulting system performance. However, performance at the 100' MDH, although improved, is still somewhat questionable. A window requirement at 100' is that the aircraft be within the $\pm.3^{\circ}$ glide slope limits (i.e., within 12 ft of the glide slope) with probability .95. Thus, the standard deviation in $H_{w=1000}$ must be less than 6 ft.† Table 1 indicates σ=8' with no turbulence. If the model were modified to include piecewise constant gains as discussed, we would predict $\sigma \simeq 4'$ which is satisfactory. However, under turbulent conditions the model predicts σ=20', and even if the gains were modified it is unlikely that the predicted σ would be less than 10'. We therefore conclude that the display is inadequate with regard to window performance at the MDH (under moderate turbulence).

Addition of Velocity Vector Symbol

No Turbulence-- In an attempt to provide the pilot with sink rate information that could be useful for control purposes, a velocity

†The 2σ point on a Gaussian distribution includes 95% of the area.

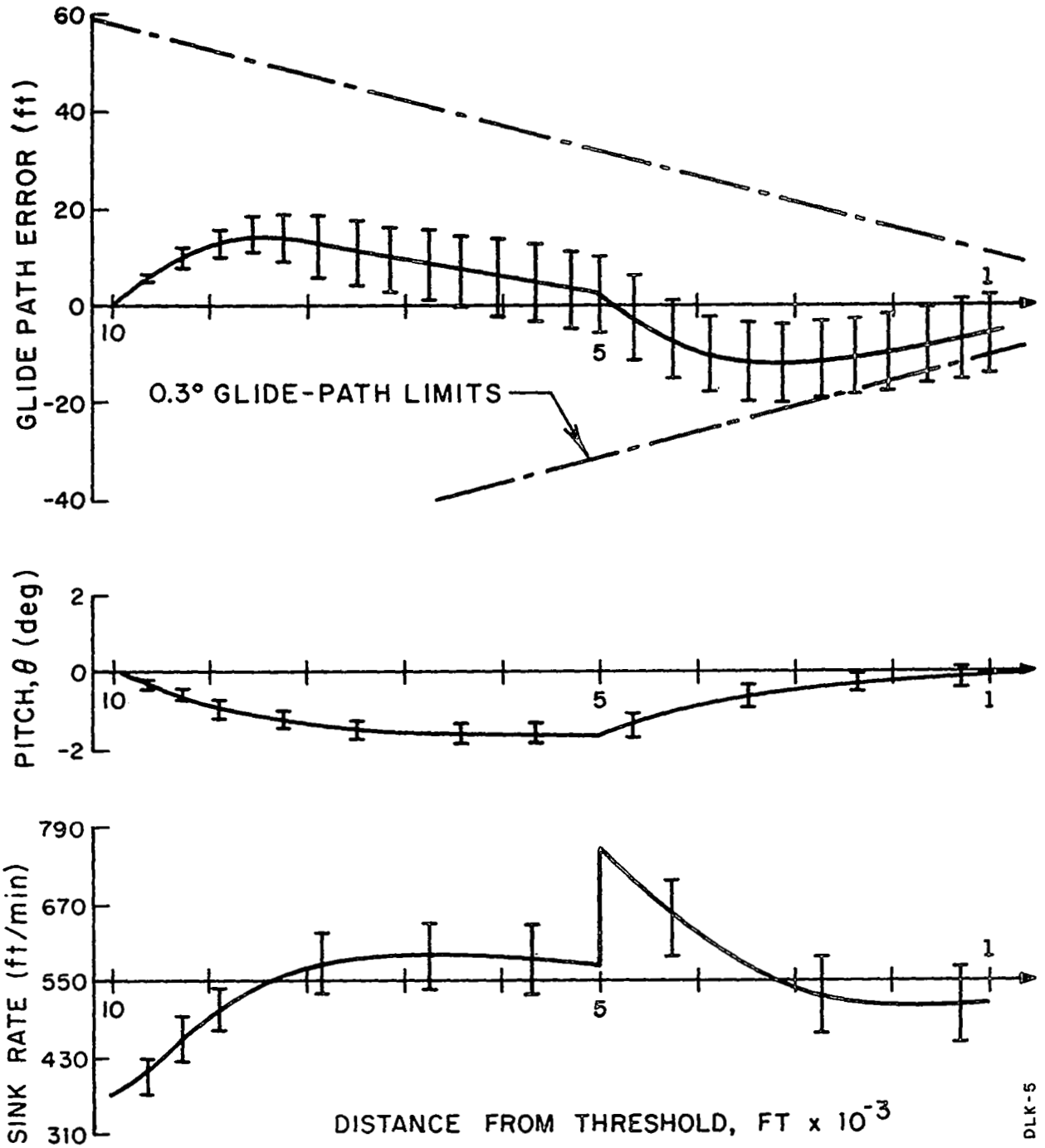

FIG. 6 PREDICTED PERFORMANCE: REFERENCE BAR AND VELOCITY VECTOR AUGMENTATION, NO TURBULENCE

vector symbol was added to the display as discussed earlier. We model this situation by including $\dot{h}(t)$ as a perceived output with -20 dB observation noise. No other model parameters change.

The predicted trajectories of $h(t)$, $\theta(t)$ and $\dot{h}(t)$ are shown in Fig. 6. The results are much the same as those in Fig. 5, with the notable difference that over R_1 the pilot responds much more quickly to the updraft. This is because the step displacement in $\dot{h}$ is observed, allowing the value of the updraft to be rapidly estimated. As a result, mean glide path deviations over R_1 are reduced. Note also that deviations of $E\{\dot{h}(t)\}$ from the nominal -550 ft/min are reduced by adding the aim point.

Predicted response over R_2 is virtually the same as that without the aim point since the pilot knows for sure that the updraft is terminated at 5000'. The aim point would be helpful if the pilot did not know this fact.

Measured and predicted means and RMS are given in Table 3. The agreement is excellent considering that measured data is the average of only 6 runs. Measured data shows the predicted improvement in $\bar{\alpha}$ over the 10-5000' range. Measured quantities over the second interval are not significantly different from those without the aim point (Table 1). This substantiates our claim that the aim point makes little difference to the longitudinal control task in the absence of constant winds and turbulence.

Predicted standard deviations in $h(t)$ at the 5000 and 1000' ranges are virtually the same as with no aim point. This indicates that the (no turbulence) probability distributions at the MDH remain unchanged. Note that measured sigmas show a 50% decrease, but this is a dubious result; only 6 runs were averaged and α measurements do not seem to indicate decreases in glide path variance.

TABLE 3

MODEL AND MEASURED PERFORMANCE:† AIM-POINT, NO TURBULENCE

	Mean (10-5000') RMS				Mean (5-1000') RMS			
	Model	Measured	Model	Measured	Model	Measured	Model	Measured
q(deg/sec)	-.06	-.06(.02)	.30	.47(.17)	.07	.08(.03)	.30	.53(.32)
θ(degrees)	-1.22	-1.11(.1)	1.34	1.24(.07)	-.57	-.83(.10)	.80	1.03(.13)
δ_e(degrees)	.29	.26(.03)	.37	.36(.04)	.46	.46(.04)	.50	.53(.04)
$-\dot{h}$(ft/min)	548.	539(9)	555.	547(9)	577.	615(16)	585.	624(15)
α(degrees)	.06	.08(.03)	.08	.09(.03)	-.14	.06(.06)	.20	.10(.05)
H_T(feet)	317	326	σ=8	σ=4	99	106	σ=8	σ=1.5

†Measured data is the average of 6 runs.

TABLE 4

MODEL AND MEASURED PERFORMANCE:† AIM-POINT, TURBULENCE

	Mean (10-5000') RMS				Mean (5-1000') RMS			
	Model	Measured	Model	Measured	Model	Measured	Model	Measured
q(deg/sec)	-.06	-.03(.03)	.79	1.09(.08)	.07	.09(.08)	.80	1.35(.28)
θ(degrees)	-1.22	-1.32(.4)	1.68	1.61(.35)	-.56	-.41(.63)	1.34	1.25(.3)
δ_e(degrees)	.29	.31(.08)	.42	.45(.06)	.46	.40(.21)	.56	.59(.16)
$-\dot{h}$(ft/min)	549.	553(36)	564.	568(33)	576.	592(52)	595.	609(49)
α(degrees)	.06	.06(.08)	.10	.11(.05)	-.14	.07(.11)	.29	.14(.08)
w_g(ft/sec)	0.0	-.3(1.2)	3.0	3.12(.32)	0.0	.77(.87)	3.0	3.57(.48)
H_T(feet)	317	322	σ=14	σ=15	99	109	σ=15	σ=5

†Measured data is the average of 6 runs.

Effects of Turbulence-- Measured and predicted quantities obtained with simulated turbulence conditions are shown in Table 4. As expected, mean response shows little change from that of the no turbulence aim-point conditions above. However, the model predicts that with moderate turbulence the addition of the aim point results in 20-30% reductions in the standard deviation of h at 5000 and 1000' and in RMS α over R_2.[†] Measured RMS α shows an improvement of 30% over the no aim-point case; measured window data is unreliable, being the average of only 6 runs.

We therefore conclude that the aim point does improve height performance at 100 ft., however the improvement is not sufficient. The model predicts the S.D. in h_{1000} to be 15'. Even if the model's feedback gains were adjusted as a function of range, it is unlikely that σ would be less than $\approx$7 ft. This is still greater than the 95% requirement of σ=6. In the conclusions we indicate some display modifications that may tighten height performance at the window.

Sensitivity Studies.— In order to gain a deeper understanding of the inter-relationship between the display and pilot behavior, we use the model to examine the effects on system performance of changes in some basic display parameters. We consider the no aim-point configuration in the absence of turbulence. The results for the nominal case are shown in Fig. 5 and Table 1.

Display Update Interval-- Delays in updating the TV image are included within the model's equivalent perceptual time-delay τ. Therefore, to investigate the sensitivity of system performance to the update interval, we varied τ from .3 to .6 sec (corresponding to update times of .1 to .4 sec). We found that model predictions were virtually insensitive to time-delay variations over

[†]Recall that in the no turbulence case these quantities were not affected by adding the aim point.

this range. This agrees with the experimental results of Wempe and Palmer [1] concerning update interval sensitivity.

The insensitivity of the system to update time is comforting. It means that the display and its accompaning software do not place high demands on real time computation.

Display Resolution-- We model degradation in display resolution as increases in observation noise. Accordingly, we simultaneously varied the observation noise ratios from -20 dB to -8 dB, a factor of 16, and computed the resulting system performance.

Figure 7 shows the mean and standard deviation of several performance measures as a function of observation noise. (RMS^2 = $mean^2$ + SD^2.) Noteworthy is that system performance is not very sensitive to observation noise over the range -20 to -14 dB. Sensitivity increases somewhat as observation noise is increased further.

Experimental results have also shown an insensitivity of performance to degradation in runway image resolution [1,2]. In the experiments of Ref.[2], measurements were made under simulated flights with 0.4° resolution, i.e., a degradation by a factor of 8. If we equate a factor of 8 in resolution with a factor of 8 in observation noise, then predictions with -11 dB noise on α should compare with the measured data.† Table 5 shows this comparison. The agreement is excellent with both model and measured data showing the same trends from the nominal -20 dB case in Table 1.

†This is a reasonable hypothesis. However, a detailed analysis of the display would require measuring observation noise as a function of resolution.

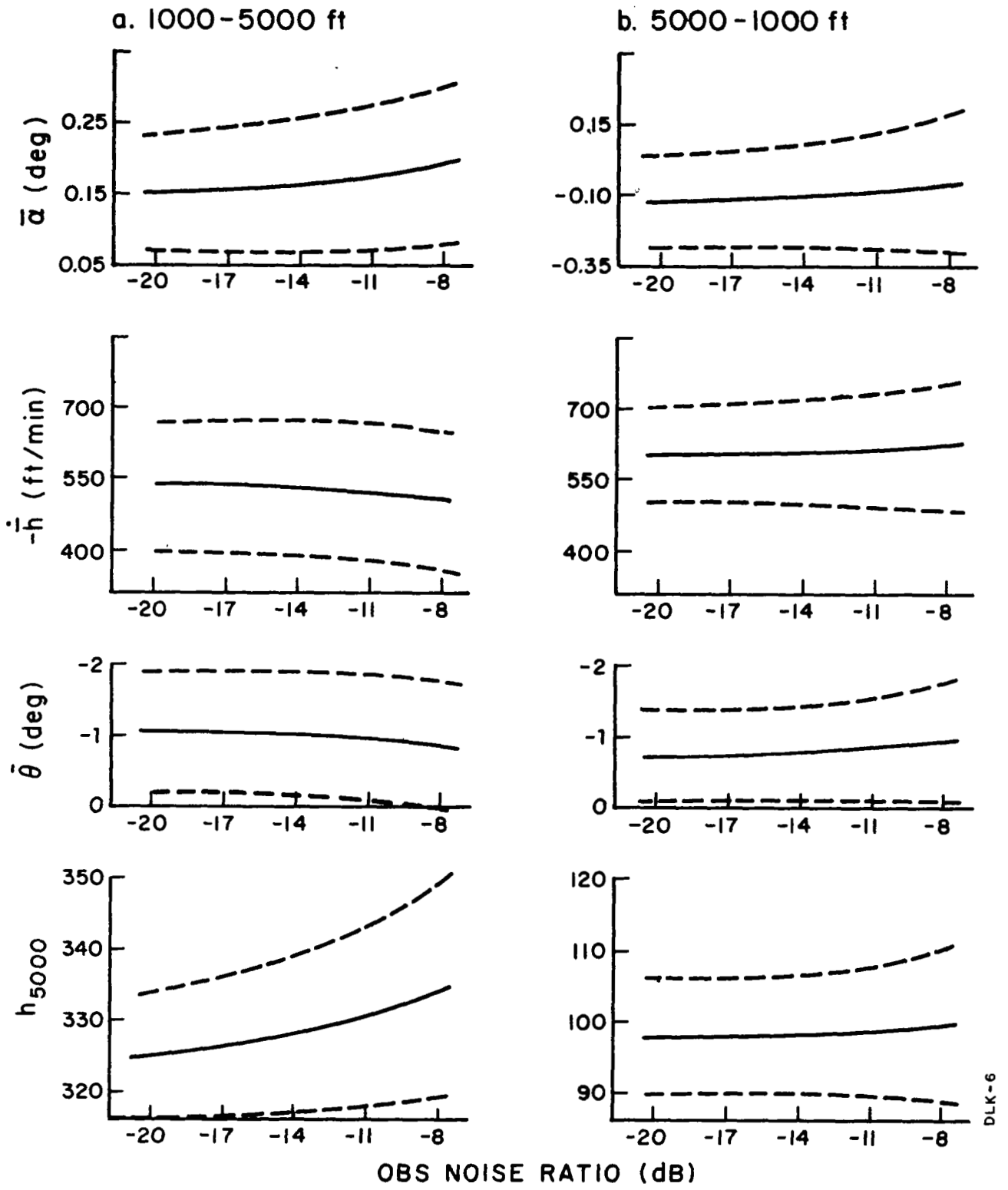

FIG. 7 EFFECTS OF OBSERVATION NOISE ON SYSTEM PERFORMANCE

TABLE 5

MODEL AND MEASURED PERFORMANCE:† REFERENCE BARS, NO TURBULENCE, DEGRADED RESOLUTION

	Mean (10-5000') RMS				Mean (5-1000') RMS			
	Model	Measured	Model	Measured	Model	Measured	Model	Measured
q(deg/sec)	-.07	-.05(.02)	.32	.34(.08)	.08	.07(.04)	.31	.40(.12)
θ(degrees)	-.97	-.86(.21)	1.33	1.08(.24)	-.81	-1.05(.2)	1.04	1.23(.18)
δ_e(degrees)	.19	.18(.06)	.31	.27(.07)	.49	.48(.03)	.53	.51(.05)
$-\dot{h}$(ft/min)	519.	505.(35)	537.	516.(34)	617.	655.(38)	628.	666.(35)
α(degrees)	.18	.17(.06)	.20	.18(.07)	-.08	.11(.13)	.22	.18(.09)
H_T(feet)	331	340	σ=13	σ=14	99	105	σ=9	σ=6

†Measured data is the average of 17 runs.

The results show that with increased observation noise it takes longer for the model to estimate the value of the updraft and less compensation is made over the 10-5000' range. The result is a lowering in mean pitch and sink rate over R_1, accompanied by an increase in mean glide path error and height error at 5000'. Over the interval R_2 pitch and sink rate increase slightly (to compensate for their decreases over R_1) and aircraft height at 1000' winds up virtually unchanged.

The system's slight sensitivity to observation noise is a desirable property. Apart from the obvious interpretation with respect to degrading the display, this insensitivity can be interpreted in terms of pilot workload and attentional demand [10]. It says that the workload demand of the task is small and that the pilot should be able to perform additional tasks (if necessary). Thus, lateral control and the inclusion of a throttle should present no difficulty to the pilot. This confirms the well-known fact that a NAVION is easy to fly.†

Display Gain-- We assume that a change in display gain will cause an inversely proportional change in the visual thresholds on displayed quantities. Thus, in the present situation, gain changes will change the glide slope threshold a_α. (For purposes of analysis we assume that this threshold is in fact visual.)

There may be other effects associated with gain variations. For example, the cost functional weighting m_α may be influenced by the display gain when the gain is relatively small. This effect is mentioned in Appendix D, however little is known of the cause.

†In cases where approach performance is sensitive to observation noise, care must be exercised in relegating additional tasks to the pilot for fear of overload. Furthermore, it is possible to show a correspondence between observation noise sensitivity and pilot rating.

and effect relationship as regards the pilot. For this reason, we neglect any such phenomena and simply assume that m_α is independent of display gain.

Figure 8 shows the mean trajectories of glide slope deviations, pitch and sink rate for an increase and a decrease in display gain by a factor of 2. Thus, $a_\alpha = .05^\circ$ and $.2^\circ$ respectively. The standard deviations about the mean are not shown as they were affected little by gain changes. The results offer no surprises. The larger the threshold, the longer is the wait before the pilot begins corrective action. The result is that larger corrections must be made over a shorter period of time to return the aircraft to the glide slope. It is clear that with no aim point, a higher display gain would be desirable.

Display gain variations were also studied for the aimpoint condition. It was found that system performance was highly insensitive to display gain. This is simply because the updraft can be determined almost immediately from $\dot{h}(t)$ information, before the aircraft has actually drifted very far off the glide slope.

DC-8 Dynamics.— Experiments using the display with velocity vector symbol included were also performed with simulated DC-8 dynamics. In order to demonstrate further the versatility and ease of use of the analysis technique, we apply the model in a straightforward manner to predict closed-loop behavior under conditions of: (i) no turbulence, $\sigma_g=0$, (ii) moderate turbulence, $\sigma_g=3.0$ and (iii) severe turbulence, $\sigma_g=6.0$.

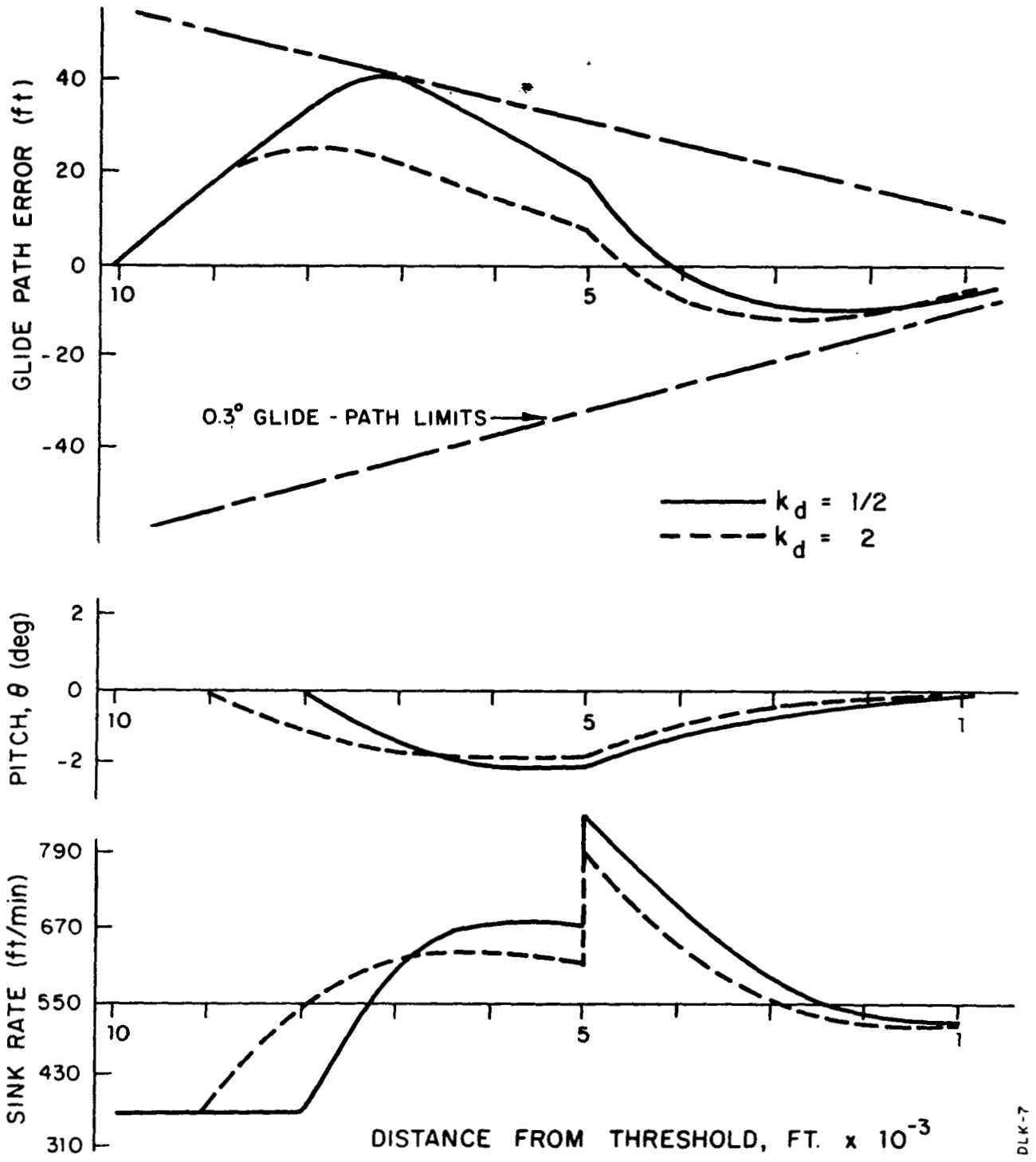

FIG. 8 MEAN RESPONSE WITH DIFFERENT DISPLAY GAINS

____ k_d = 1/2 ---- k_d = 2

The stability derivatives pertinent to the DC-8 are

$X_u = -.283 \text{ sec}^{-1}$ $\quad M_u = 0$

$X_w = .136 \text{ sec}^{-1}$ $\quad M_w = -.264 \text{ deg/ft-sec}$

$Z_u = -.283 \text{ sec}^{-1}$ $\quad M_q = -.594 \text{ sec}^{-1}$

$Z_w = -.75 \text{ sec}^{-1}$ $\quad M_\delta = -.923 \text{ sec}^{-2}$

$Z_\delta = -.1618 \text{ ft-sec}^{-2}/\text{deg}$ $\quad U_o = 229/57.3 = 4.0 \text{ ft-sec}^{-1}/\text{deg}$

The glide slope conditions that we consider are identical to those for the NAVION. The only difference is the nominal sink rate which now becomes -11.99 ft/sec.

The application of the model is straightforward: We assume that the various parameters that quantify the pilot's limitations and the display characteristics are invariant to changes in vehicle dynamics.† We also assume that the cost functional weightings m_α and m_q remain unchanged. This latter assumption is not necessarily true. However, for the given task we felt that the relative weightings used for the NAVION (i.e., $m_\alpha/m_q = .5$) were also reasonable for the DC-8. Thus, our initial choice was

$$m_h = .005, \; m_q = 1, \; m_{\dot{\delta}_c} = .017$$

which resulted in $\tau_N = .1$ sec.

Figure 9 shows the trajectories (mean and SD) of glide-path errors, pitch and sink rate corresponding to $\sigma_g = 3.0$ ft/sec. The trajectories are similar to those in Fig. 6. Note, also

†Display gain was reduced by 2, so that we take $a_\alpha = .2$.

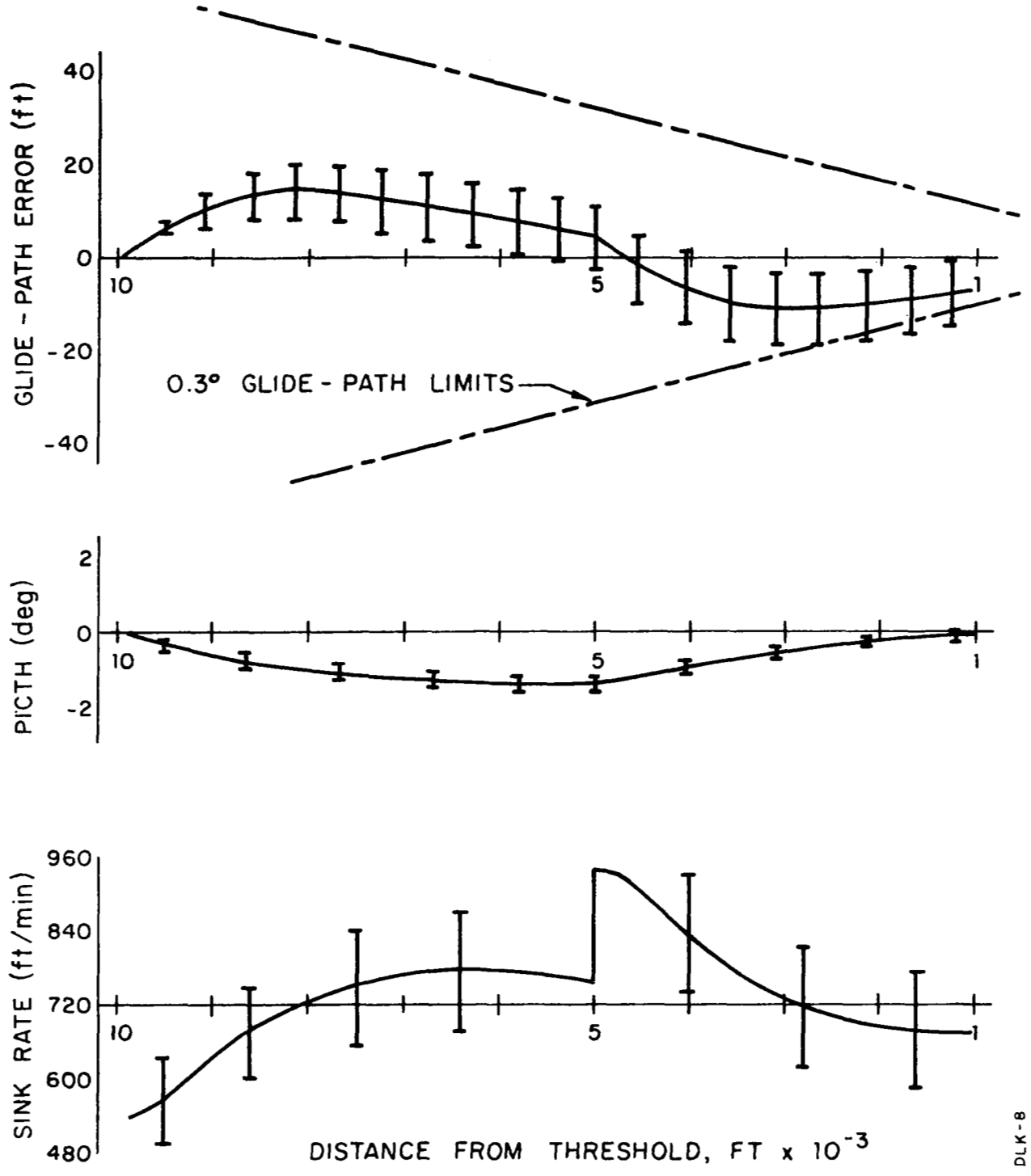

FIG. 9 PREDICTED PERFORMANCE: DC-8, AIM POINT DISPLAY, TURBULENCE

that the predicted glide-path variability is very much the same. Figure 6 corresponds to σ_g=0 while Fig. 8 has σ_g=3.0, yet the standard deviations of h(t) about its mean are approximately equal. This implies that the display should be satisfactory for a DC-8 under moderate turbulence. (A DC-8 simply doesn't "bounce around" much in this case.)

Table 6 gives averaged RMS performance over the intervals R_1 and R_2 for the different turbulence levels. Mean performance is unaffected by the gusts. The results clearly show the increase in RMS with increasing σ_g. For σ_g=6.0, the standard deviation in h(t) at 1000' is 14.5 ft. This spread is unsatisfactory with regard to window requirements. Even if the control gains were adjusted with range, it is highly unlikely that the predicted SD would be less than 7 ft.

TABLE 6

PREDICTED PERFORMANCE: DC-8 DYNAMICS, AIM POINT, TURBULENCE

	Mean	RMS (10-5000')			Mean	RMS (5000-1000')		
		σ_g=0	σ_g=3	σ_g=6		σ_g=0	σ_g=3	σ_g=6
q (deg/sec)	-.07	.09	.20	.36	.07	.10	.21	.37
θ (degrees)	-1.0	1.08	1.14	1.29	-.58	.69	.80	1.06
δ_e(degrees)	.41	.47	.69	1.12	.49	.53	.74	1.17
$-\dot{h}$ (ft/min)	709	714	719	737	761	766	773	794
α (degrees)	.07	.07	.08	.11	-.13	.16	.20	.29
H_T(feet)	319	σ=2	σ=7.5	σ=14.5	98	σ=2	σ=7.5	σ=14.5

CONCLUDING REMARKS

A computerized pilot-vehicle-display systems model has been applied to the evaluation of a pictorial display for approach to landing. This display is under investigation at Ames Research Center in connection with potential independent, landing monitor display systems. The analysis focused on determining the effects of display changes on closed-loop performance. The results of adding two types of guidance symbology and of changing display resolution, update interval and gain were predicted.

On the basis of the predicted results, we can conclude that the basic pictorial display with augmented glide slope reference bars and aim point symbology, provides for adequate longitudinal approach performance in calm air. The "pilot" can control the aircraft to within the glide slope tolerances in the presence of vertical updrafts. The updrafts are quickly estimated by the model and are "trimmed out" accordingly.

Under moderate turbulence, the display appears to be adequate for a DC-8 approach but not for a light aircraft. Standard deviations in height at the decision window exceed the desired 95% tolerance.

Are there methods for improving the display still further? This question is nontrivial but it may be answered in part by using the model to investigate the effects of additional information (e.g., velocity information), using a "quickened" display, and other modifications. On the basis of our analysis, however, it appears that a doubling of display gain coupled with a reduction in the width of the glide slope reference bars (i.e., to $\pm.15^{o}$)

should improve height performance. The reason is that the cost functional weighting on glide path errors should increase and as a result the RMS errors should decrease (although pilot workload may increase!)

There are other factors that point to improved performance with the display in a real aircraft. Use of a throttle control should help to reduce glide path variability. The lack of throttle control is, to some extent, unrealistic and may account for some of the observed variability. In addition, the use of a trim wheel should reduce RMS errors. Pilot induced motor noise scales with the control input. If the control has a mean or trim component, use of a trim tab frees the pilot from holding a constant control and thereby reduces pilot remnant. The result is a lowering of system variability.

Of prime importance in the analytical display evaluation procedure was an optimal-control model for the human pilot. This model allowed us to calculate various aspects of closed-loop performance as a function of changes in the display. The basic pilot-model was developed prior to this investigation. However, in the course of this effort the model was broadened to include time-varying sensing and information processing characteristics, response to deterministic inputs and visual/indifference thresholds.

A secondary objective of this effort was to evaluate the extended version of the model that we had developed. Accordingly, predictions were compared with data obtained in the Ames experiments. The comparisons revealed a remarkable agreement between model and measured data across all measurement dimensions. Mean and RMS scores demonstrate the model's ability to predict both the time-varying adaptability of a "pilot" as well as the effects

of "his" randomness. It is noteworthy that predictions were obtained with model parameter values equal to those that have been measured in independent, basic manual control experiments.

Some further extensions to the model suggest themselves. The most important of these appear to be the addition of time-varying gains and the continuation of the flight path through flare and rollout. The adaptability and validity of the model's structure as demonstrated by the results of this effort give us confidence that these improvements can be accomplished.

REFERENCES

1. Wempe, T. and Palmer, E., "Pilot Performance with a Simulated Pictorial Landing Display Including Different Conditions of Resolution and Update Rate," Proceedings of the Sixth Annual Conference on Manual Control, Wright-Patterson Air Force Base, Ohio, April 1970.

2. Palmer, E. and Wempe, T., "Pilot Performance with a Simulated Augmented Pictorial Landing Display," Proceedings of the Seventh Annual Conference on Manual Control, UCLA, Los Angeles, California, May 1971. (to be presented)

3. Kleinman, D.L., Baron, S. and Levison, W.H., "An Optimal Control Model of Human Response, Parts 1 and 2", Automatica, Vol. 6, May 1970.

4. Kleinman, D.L. and Baron, S., "Manned Vehicle Systems Analysis by Means of Modern Control Theory," BBN Report No. 1967, Bolt Beranek and Newman Inc., Cambridge, Massachusetts, June 1970.

5. Rynaskii, E.G. and Whitbeck, R.F., "The Theory and Application of Linear Optimal Control," AFFDL-TR-65-28, January 1966.

6. Levison, W.H., Baron, S. and Kleinman, D.L., "A Model for Human Controller Remnant," IEEE Trans. Man-Machine Systems, Vol. MMS-10, No. 4, December 1969.

7. Kleinman, D.L., "Optimal Control of Linear Systems with Time-Delay and Observation Noise," IEEE Trans Autom. Control, Vol. AC-14, No. 5, October 1969.

8. Athans, M. and Falb, P., Optimal Control: An Introduction to the Theory and its Applications, McGraw-Hill Book Co., New York, 1966.

9. Kleinman, D.L., Fortmann, T., and Athans, M., "On the Design of Linear Systems with Piecewise-Constant Feedback Gains," IEEE, Trans. Autom. Control, Vol. AC-13, No. 4, August 1968.

10. Levison, W.H., "Studies of Multivariable Manual Control Systems: A Model for Task Interference," BBN Report 1892, Bolt Beranek and Newman Inc., Cambridge, Massachusetts, December 1969.

11. Johnson, C.D., "Optimal Control of the Linear Regulator with Constant Disturbances," IEEE Trans. Autom. Control, Vol. AC-13, No. 4, August 1968.

12. Bongiorno, J.J. and Youla, D.C., "On Observers in Multivariable Control Systems," Int. J. of Control, Vol. 8, Sept. 1968.

13. McRuer, D.T. and Krendel, E.S., "Dynamic Response of Human Operators," Wright Air Dev. Center, WADC TR56-524, Wright-Patterson Air Force Base, Ohio, October 1957.

14. Graham, D. and McRuer, D.T., Analysis of Nonlinear Control Systems, John Wiley and Sons, Inc., New York, 1961.

15. Booton, R.C., "Nonlinear Control Systems with Random Inputs," IRE Trans. Circuit Theory, Vol. CT-1, 1954.

16. Levison, W.H., "The Effects of Display Gain and Signal Bandwidth on Human Controller Remnant," BBN Report 1968, Bolt Beranek and Newman Inc., Cambridge, Massachusetts, August 1970.

APPENDIX A

OPTIMIZATION WITH CONSTANT INPUT DISTURBANCES

In this section we investigate the optimal control of linear systems that are subject to constant external disturbances. Such is the case in aircraft approach when a constant updraft or cross-wind is present.

Problem Formulation

The system being considered is defined by the state equations

$$\dot{\underline{x}}(t) = \underline{A}\ \underline{x}(t) + \underline{B}\ \underline{u}(t) + \underline{\gamma}\ w_o + \underline{w}(t) \qquad \text{(A-1)}$$

where $\underline{x}(t)$ and $\underline{u}(t)$ are the vehicle's state and control input, respectively. w_o represents a known, constant, disturbance.† $\underline{w}(t)$ models external, random disturbances and is assumed to be white-noise.

The control objective is to choose $\underline{u}(t)$ that minimizes the cost functional

$$J(\underline{u}) = \lim_{T\to\infty} E\left\{\frac{1}{T}\int_0^T [\underline{x}'(t)\underline{Q}\ \underline{x}(t) + \underline{u}'(t)\underline{R}\ \underline{u}(t)]dt\right\} \qquad \text{(A-2)}$$

†In actuality, w_o is the best estimate of the constant disturbance. This estimate is generated by a Kalman filter, or by a Luenberger "observer". This point is relatively unimportant in the present context since all states will require estimation and Eq.(A-1) will define the estimator. For a further study of linear systems subject to constant external disturbances, see Ref.[11].

Problem Solution

In order to solve the above problem we define an additional state $x_{n+1}(t) = w_o$. Thus

$$\dot{x}_{n+1}(t) = 0,$$

and the equation (A-1) may be written

$$\dot{\tilde{\underline{x}}}(t) = \tilde{\underline{A}}\,\tilde{\underline{x}}(t) + \tilde{\underline{B}}\,\underline{u}(t) + \tilde{\underline{w}}(t) \qquad \text{(A-3)}$$

where $\tilde{\underline{x}} = \text{col}(\underline{x}, x_{n+1})$, $\tilde{\underline{w}} = \text{col}(\underline{w}, 0)$ and

$$\tilde{\underline{A}} = \left[\begin{array}{c|c} \underline{A} & \underline{\gamma} \\ \hline \underline{0} & 0 \end{array}\right] \qquad \tilde{\underline{B}} = \left[\begin{array}{c} \underline{B} \\ \hline \underline{0} \end{array}\right]$$

The $\underline{x}$-related term in the cost functional $J(\underline{u})$ thus becomes

$$\underline{x}'(t)\underline{Q}\,\underline{x}(t) = \tilde{\underline{x}}'(t)\tilde{\underline{Q}}\,\tilde{\underline{x}}(t)$$

where

$$\tilde{\underline{Q}} = \left[\begin{array}{c|c} \underline{Q} & \underline{0} \\ \hline \underline{0} & 0 \end{array}\right]$$

Let us now consider a fixed value of T. The minimization of $J(\underline{u})$ subject to the dynamic constraint (A-3) is therefore a well-defined linear optimal regulator problem. The optimal control is given by

$$\underline{u}(t) = - \underline{R}^{-1}\underline{\tilde{B}}'\underline{\tilde{K}}(t)\ \underline{\tilde{x}}(t) = - \underline{L}^{*}(t)\ \underline{\tilde{x}}(t) \qquad \text{(A-4)}$$

where $\underline{\tilde{K}}(t)$ is the solution of the Riccati equation

$$- \dot{\underline{\tilde{K}}}(t) = \underline{\tilde{K}}(t)\underline{\tilde{A}} + \underline{\tilde{A}}'\underline{\tilde{K}}(t) + \underline{\tilde{Q}} - \underline{\tilde{K}}(t)\underline{\tilde{B}}\ \underline{R}^{-1}\underline{\tilde{B}}'\underline{\tilde{K}}(t),\ t \leq T$$

$$\underline{\tilde{K}}(T) = \underline{0} \qquad \text{(A-5)}$$

If we now write

$$\underline{\tilde{K}} = \left[\begin{array}{c|c} \underline{K}_{11} & \underline{k}_{12} \\ \hline \underline{k}'_{12} & k_{22} \end{array}\right]$$

and substitute into Eq. (A-4), $\underline{u}(t)$ may be written

$$\underline{u}(t) = - \underline{R}^{-1}\underline{B}'\underline{K}_{11}(t)\ \underline{x}(t) - \underline{R}^{-1}\underline{B}'\underline{k}_{12}(t)w_o$$

$$= - \underline{L}_1(t)\ \underline{x}(t) - \underline{L}_2(t)w_o$$

From Eq. (A-5), the partitions $\underline{K}_{11}$ and $\underline{k}_{12}$ satisfy

$$\begin{aligned} - \dot{\underline{K}}_{11}(t) &= \underline{K}_{11}\underline{A} + \underline{A}'\underline{K}_{11} + \underline{Q} - \underline{K}_{11}\underline{B}\ \underline{R}^{-1}\underline{B}'\underline{K}_{11}; \\ \underline{K}_{11}(T) &= \underline{0} \end{aligned} \qquad \text{(A-6)}$$

$$-\dot{\underline{k}}_{12} = \underline{K}_{11}\underline{\gamma} + (\underline{A}-\underline{B}\ \underline{R}^{-1}\underline{B}'\underline{K}_{11})'k_{12};\quad \underline{k}_{12}(T) = \underline{0} \qquad (A-7)$$

Note that $\underline{K}_{11}$ is independent of $\underline{k}_{12}$; both $\underline{K}_{11}$ and $\underline{k}_{12}$ are independent of k_{22}. Thus $\underline{L}_1$ are the optimal feedback gains in the absence of constant disturbances.

We now let $T \to \infty$ to determine the "steady-state" feedback gains. It is well-known [8] that as $T \to \infty$ in Eq. (A-6) the solution $\underline{K}_{11}(t)$ approaches $\overline{\underline{K}}$ which is the unique positive-definite solution of the algebraic equation

$$\underline{0} = \overline{\underline{K}}\ \underline{A} + \underline{A}'\overline{\underline{K}} + \underline{Q} - \overline{\underline{K}}\ \underline{B}\ \underline{R}^{-1}\underline{B}'\overline{\underline{K}} \qquad (A-8)$$

In addition, the "closed-loop" matrix

$$\overline{\underline{A}} = \underline{A} - \underline{B}\underline{R}^{-1}\underline{B}'\overline{\underline{K}}$$

has eigenvalues with negative real parts. Using this fact, it can be shown that

$$\overline{\underline{k}}_{12} = \lim_{T\to\infty} \underline{k}_{12}(t) = -(\overline{\underline{A}}^{-1})'\underline{K}\ \underline{\gamma} \qquad (A-9)$$

Thus, the control that minimizes $J(\underline{u})$ is

$$\begin{aligned}\underline{u}(t) &= -\underline{R}^{-1}\underline{B}'\overline{\underline{K}}\ \underline{x}(t) + \underline{R}^{-1}\underline{B}'(\overline{\underline{A}}^{-1})'\overline{\underline{K}}\ \underline{\gamma}\ w_o \\ &= -\underline{L}_1\ \underline{x}(t) - \underline{L}_2\ w_o\end{aligned} \qquad (A-10)$$

Properties of Solution

The optimal control (A-10) consists of two parts. As already noted, the first part represents the optimal control in the absence of w_o. The second term is a constant $\underline{u}_o$ that scales with w_o and assures correct system adaptation to the external disturbance. It is instructive to investigate the mean response, i.e., $E\{\underline{x}(t)\} = \bar{\underline{x}}$, and the corresponding mean control input

$$\bar{\underline{u}} = - \underline{L}_1 \bar{\underline{x}} - \underline{L}_2 w_o = - \underline{L}_1 \bar{\underline{x}} + \underline{u}_o \qquad \text{(A-11)}$$

We can show the following:

Lemma: 1) $\bar{\underline{u}}$ is such that the system (A-1) is in equilibrium, i.e., $\dot{\bar{\underline{x}}} = \underline{0}$.

2) $\underline{u}_o$ is such that $\bar{\underline{u}} = - \underline{L}_1 \bar{\underline{x}} + \underline{u}_o$ minimizes

$$J(\bar{\underline{u}}) = \bar{\underline{x}}' \underline{Q}\, \bar{\underline{x}} + \bar{\underline{u}}' \underline{R}\, \bar{\underline{u}} \qquad \text{(A-12)}$$

Proof: 1) From Eq. (A-1)

$$\dot{\bar{\underline{x}}} = \underline{\bar{A}}\, \bar{\underline{x}} + \underline{B}\, \underline{u}_o + \underline{\gamma}\, w_o$$

but since $\underline{\bar{A}}$ is a stable matrix, $\dot{\bar{\underline{x}}} \to \underline{0}$ as $t \to \infty$. Thus

$$\bar{\underline{x}} = - \underline{\bar{A}}^{-1} (\underline{B}\, \underline{u}_o + \underline{\gamma}\, w_o)$$

2) To show the optimality of $\underline{u}_o$, substitute $\bar{\underline{u}}$ into $J(\bar{\underline{u}})$ to obtain

$$J(\bar{u}) = \bar{x}'(Q + \bar{K}\,B\,R^{-1}B'\bar{K})\bar{x} - 2\bar{x}'\bar{K}\,B\,u_o + u_o'R\,u_o$$

$$= -2\bar{x}'\bar{K}\,\bar{A}\,\bar{x} - 2\bar{x}'\bar{K}\,B\,u_o + u_o'R\,u_o$$

$$= -2\bar{x}'\bar{K}(\bar{A}\,\bar{x} + B\,u_o) + u_o'R\,u_o$$

Since $\bar{x}$ depends on u_o, we substitute to obtain

$$J(\bar{u}) = u_o'R\,u_o - 2\gamma'w_o(\bar{A}^{-1})'\bar{K}\,\gamma\,w_o - 2u_o'B'(\bar{A}^{-1})'\bar{K}\,\gamma\,w_o$$

Differentiating with respect to u_o gives

$$\frac{\partial J}{\partial u_o} = 0 = 2R\,u_o - 2B'(\bar{A}^{-1})'\bar{K}\,\gamma\,w_o$$

or

$$u_o = R^{-1}B'(\bar{A}^{-1})'\bar{K}\,\gamma\,w_o \qquad \text{(A-13)}$$

which is the desired result. Thus the system chooses a constant input† to adjust the system states in an optimal way to offset the effects of w_o. QED

In the above analysis, w_o was assumed known. However, the optimal feedback gains L_1 and L_2 were found to be independent of the value of w_o. Thus the control law (A-10) will be optimal for any w_o. When w_o is unknown, we simply replace w_o by its best estimate $\hat{w}_o(t)$. Since $\dot{w}_o = 0$, the estimate $\hat{w}_o(t)$ i independent of $\hat{w}_o(\sigma)$ for $\sigma < t$, and is used in the feedback loop

†i.e., a "trim condition".

in lieu of w_o. The estimate $\hat{w}_o$ can be generated from $\underline{x}(t)$ by an "observer" that has arbitrary dynamics [12]. In fact, the estimate $\hat{w}_o$ can be made to approach w_o arbitrarily fast, i.e.,

$$\hat{w}_o(t) \rightarrow w_o$$

Furthermore, if $x_1, x_2, \ldots x_n$ are available to the feedback system, then w_o can be estimated arbitrarily fast with a first order system [12].

APPENDIX B

OPTIMIZATION WITH TIME-VARYING OBSERVATION NOISE

One of the facets of the aircraft approach problem is that the observation noises associated with altitude related quantities decrease monotonically with absolute altitude (or distance from touchdown). This non-stationarity requires a slight modification of our earlier results dealing with optimization in the presence of time-delay and (stationary) observation noise [7]. In this section we present the new results.

Problem Formulation

The vehicle is assumed to be described by the state-output equations

$$\dot{\underline{x}}(t) = \underline{A}\ \underline{x}(t) + \underline{B}\ \underline{u}(t) + \underline{w}(t) \qquad \text{(B-1)}$$

$$\underline{y}(t) = \underline{C}(t)\ \underline{x}(t-\tau) + \underline{v}(t-\tau) \quad ; \quad \tau \geq 0 \qquad \text{(B-2)}$$

$\underline{A}$ and $\underline{B}$ are constant, but $\underline{C}$ may be time-varying, thereby reflecting outputs that vary with time. The driving noise $\underline{w}(t)$ and the observation noise $\underline{v}(t)$ are non-stationary, independent, white Gaussian noises with autocovariance matrices

$$E\{\underline{w}(t)\ \underline{w}'(\sigma)\} = \underline{W}(t)\ \delta(t-\sigma) \qquad \text{(B-3)}$$

$$E\{\underline{v}(t)\ \underline{v}'(\sigma)\} = \underline{V}(t)\ \delta(t-\sigma) \qquad \text{(B-4)}$$

We assume that $\underline{x}(t=0)$ is random with mean and variance

$$E\{\underline{x}(0)\} = \underline{0} \tag{B-5}$$

$$E\{\underline{x}(0)\ \underline{x}'(0)\} = \underline{X}_o$$

Our objective is to determine the nonanticipative control input that minimizes the cost functional

$$J(\underline{u}) = \lim_{T\to\infty} \frac{1}{T} E\left\{\int_0^T [\underline{x}'(t)\underline{Q}\ \underline{x}(t) + \underline{u}'(t)\underline{R}\ \underline{u}(t)]dt\right\}$$

conditioned on the noisy, delayed information (B-2). In addition we desire a closed-form expression for the state covariance

$$E\{\underline{x}(t)\ \underline{x}'(t)\} \triangleq \underline{X}(t)$$

Problem Solution

It is easy to apply the techniques developed in [7] (which apply to the stationary case) to the present problem. The optimal control is given by

$$\underline{u}(t) = -\underline{R}^{-1}\ \underline{B}'\overline{\underline{K}}\ \hat{\underline{x}}(t) = -\ \underline{L}^*\ \hat{\underline{x}}(t) \tag{B-6}$$

where $\overline{\underline{K}}$ is determined from the matrix Riccati Equation

$$\underline{0} = \overline{\underline{K}}\ \underline{A} + \underline{A}'\overline{\underline{K}} + \underline{Q} - \overline{\underline{K}}\ \underline{B}\ \underline{R}^{-1}\ \underline{B}'\ \overline{\underline{K}} \tag{B-7}$$

ans where $\hat{\underline{x}}(t)$ is the least-mean-square estimate of the system state $\underline{x}(t)$. $\hat{\underline{x}}(t)$ is generated by a cascade combination of a Kalman filter and a linear predictor. The Kalman filter generates a least-mean-square estimate of the delayed state $\underline{x}(t-\tau)$ according to

$$\dot{\hat{\underline{x}}}(t-\tau) = \underline{A}\,\hat{\underline{x}}(t-\tau) + \underline{\Sigma}(t-\tau)\underline{C}'(t-\tau)\underline{V}^{-1}(t-\tau)[\underline{y}(t)-\underline{C}(t-\tau)\hat{\underline{x}}(t-\tau)]$$

$$+ \underline{B}\,\underline{u}(t-\tau) \qquad \text{(B-8)}$$

$$\hat{\underline{x}}(0) = E\{\underline{x}(0)\} = \underline{0}$$

where the estimation error covariance matrix $\underline{\Sigma}(h) = E\{\underline{e}(h)\underline{e}'(h)\}$ satisfies

$$\dot{\underline{\Sigma}}(h) = \underline{A}\,\underline{\Sigma}(h) + \underline{\Sigma}(h)\underline{A}' + \underline{W}(h) - \underline{\Sigma}(h)\underline{C}'(h)\underline{V}^{-1}(h)\underline{C}(h)\underline{\Sigma}(h) \qquad \text{(B-9)}$$

$$\underline{\Sigma}(0) = \underline{X}_o$$

The predictor generates the best estimate $\hat{\underline{x}}(t)$ of the <u>current</u> state from $\underline{\rho}(t) = \hat{\underline{x}}(t-\tau)$ by

$$\hat{\underline{x}}(t) = \underline{\xi}(t) + e^{\underline{A}\tau}\,[\underline{\rho}(t) - \underline{\xi}(t-\tau)] \qquad \text{(B-10)}$$

$$\dot{\underline{\xi}}(t) = \underline{A}\,\underline{\xi}(t) + \underline{B}\,\underline{u}(t) \qquad \text{(B-11)}$$

A useful equation associated with $\hat{\underline{x}}(t)$ can be found by differentiating (B-10) and substituting (B-11) and (B-8). The result is

$$\dot{\hat{\underline{x}}}(t) = \underline{A}\,\hat{\underline{x}}(t) + \underline{B}\,\underline{u}(t) + e^{\underline{A}\tau}\,[\underline{y}(t) - \underline{C}(t-\tau)\,\underline{\rho}(t)] \quad t \geq \tau \qquad \text{(B-12)}$$

However, the term $\underline{y}(t) - \underline{C}(t-\tau)\,\underline{\rho}(t)$ can be represented by a white-noise $\underline{\tilde{W}}(t-\tau)$ with autocovariance given by

$$E\{\underline{\tilde{W}}(\alpha)\underline{\tilde{W}}'(\beta)\} = \underline{\Sigma}(\alpha)\underline{C}'(\alpha)\underline{V}^{-1}(\alpha)\underline{C}(\alpha)\underline{\Sigma}(\alpha)\delta(\alpha-\beta) \qquad \text{(B-13)}$$

In order to find a closed-form expression for $\underline{X}(t)$ we note that $\underline{x}(t)$ may be written

$$\underline{x}(t) = \hat{\underline{x}}(t) + \underline{e}_1(t) + \underline{e}_2(t)$$

where $\underline{e}_1(t-\tau)$ is the error associated with estimating $\hat{\underline{x}}(t-\tau)$, i.e., $\underline{e}_1(t-\tau) = \underline{x}(t-\tau) - \hat{\underline{x}}(t-\tau)$, and $\underline{e}_1(t-\tau)$ satisfies

$$\dot{\underline{e}}_1(t-\tau) = (\underline{A}-\underline{\Sigma}\ \underline{C}'\underline{V}^{-1}\underline{C})\underline{e}_1(t-\tau) - \underline{\Sigma C}'\underline{V}^{-1}\underline{v}(t-\tau) + \underline{w}(t-\tau) \qquad \text{(B-14)}$$

where $\underline{\Sigma} = \underline{\Sigma}(t-\tau)$, etc.

$\underline{e}_2(t)$ is the error associated with predicting $\hat{\underline{x}}(t)$ from $\hat{\underline{x}}(t-\tau)$; it is given by

$$\underline{e}_2(t) = \int_t^{t+\tau} e^{\underline{A}(t+\tau-\sigma)}\hat{\underline{w}}(\sigma-\tau)d\sigma = \int_0^{\tau} e^{\underline{A}\xi}\ \hat{\underline{w}}(t-\xi)d\xi \qquad \text{(B-15)}$$

Finally, $\hat{\underline{x}}(t)$ is given by Eq. (B-12).

Since $\hat{\underline{x}}(t)$, $\underline{e}_1(t)$ and $\underline{e}_2(t)$ are all independent of one another by virtue of Gaussianness and the properties of least-mean-square estimation, we obtain for $t \geq \tau$,

$$E\{\underline{x}(t)\underline{x}'(t)\} = E\{\hat{\underline{x}}(t)\hat{\underline{x}}'(t)\} + E\{\underline{e}_1(t)\underline{e}_1'(t)\} + E\{\underline{e}_2(t)\underline{e}_2'(t)\}$$

Since $E\{\underline{e}_1(t)\underline{e}_1'(t)\} = \underline{\Sigma}(t)$ and

$$\begin{aligned} E\{\underline{e}_2(t)\underline{e}_2'(t)\} &= \int_0^\tau e^{\underline{A}\xi}\, \underline{\Sigma}(t-\xi)\underline{C}'\underline{V}^{-1}\underline{C}\, \underline{\Sigma}(t-\xi)\, e^{\underline{A}'\xi} d\xi \\ &= \int_0^\tau e^{\underline{A}\xi}[\underline{A}\,\underline{\Sigma} + \underline{\Sigma}\,\underline{A}' - \dot{\underline{\Sigma}} + \underline{W}(t-\xi)]\, e^{\underline{A}'\xi} d\xi \\ &= \frac{d}{d\xi}\int_0^\tau e^{\underline{A}\xi}\underline{\Sigma}(t-\xi)\, e^{\underline{A}'\xi} d\xi + \int_0^\tau e^{\underline{A}\xi}\underline{W}(t-\xi)\, e^{\underline{A}'\xi} d\xi \\ &= e^{\underline{A}\tau}\, \underline{\Sigma}(t-\tau)\, e^{\underline{A}'\tau} - \underline{\Sigma}(t) \end{aligned} \tag{B-16}$$

We obtain

$$\begin{aligned} E\{\underline{x}(t)\underline{x}'(t)\} &= e^{\underline{A}\tau}\underline{\Sigma}(t-\tau)e^{\underline{A}'\tau} + \int_0^\tau e^{\underline{A}\xi}\underline{W}(t-\xi)e^{\underline{A}'\xi} d\xi \\ &\quad + e^{\overline{\underline{A}}(t-\tau)}\, \hat{\underline{X}}(\tau)e^{\overline{\underline{A}}'(t-\tau)} \\ &\quad + \int_\tau^t e^{\overline{\underline{A}}(t-\xi)}e^{\underline{A}\tau}\underline{\Sigma}(\xi-\tau)\underline{C}'\underline{V}^{-1}\underline{C}\, \underline{\Sigma}(\xi-\tau)e^{\underline{A}'\tau}e^{\overline{\underline{A}}'(t-\xi)} d\xi \end{aligned} \tag{B-17}$$

as our final result.

APPENDIX C

EFFECTS OF MEAN DISTURBANCES ON SYSTEM PERFORMANCE

In this section we investigate the estimation and control processes that are associated with initial disturbances present in the optimal closed-loop system. For simplicity we consider the no-delay ($\tau=0$) case and derive closed-form expressions for the mean and covariance of pertinent system variables.

The equations that govern the motion of the optimal closed-loop system are

$$\dot{\underline{x}}(t) = \underline{A}\underline{x}(t) - \underline{B}\ \underline{L}\ \hat{\underline{x}}(t) + \underline{w}(t) \tag{C-1}$$

$$\dot{\hat{\underline{x}}}(t) = \bar{\underline{A}}\ \hat{\underline{x}}(t) + \underline{\Sigma}(t)\underline{C}'\underline{V}^{-1}[\underline{C}\ \underline{e}(t) + \underline{v}(t)] \tag{C-2}$$

$$\dot{\underline{e}}(t) = (\underline{A} - \underline{\Sigma}\ \underline{C}'\underline{V}^{-1}\underline{C})\underline{e}(t) - \underline{\Sigma}\ \underline{C}'\underline{V}^{-1}\underline{v}(t) + \underline{w}(t) \tag{C-3}$$

where $\underline{e}(t) = \underline{x}(t) - \hat{\underline{x}}(t)$ is the estimation error, and $\bar{\underline{A}} = \underline{A} - \underline{B}\ \underline{L}$.

We assume that the initial disturbance $\underline{x}(0)$ is random with zero-mean and covariance

$$E\{\underline{x}(0)\ \underline{x}'(0)\} = \underline{\sigma}\ \underline{\sigma}' \tag{C-4}$$

Under this condition, the matrix $\underline{\Sigma}(t)$ is precomputed according to

$$\dot{\underline{\Sigma}} = (\underline{A}-\underline{\Sigma}\ \underline{C}'\underline{V}^{-1}\underline{C})\underline{\Sigma} + \underline{\Sigma}(\underline{A}-\underline{\Sigma}\ \underline{C}'\underline{V}^{-1}\underline{C})' + \underline{\Sigma}\ \underline{C}'\underline{V}^{-1}\underline{C}\ \underline{\Sigma} + \underline{W} \tag{C-5}$$

$$\underline{\Sigma}(0) = \underline{\Sigma}_o + \underline{\sigma}\ \underline{\sigma}'$$

where $\underline{\Sigma}_o$ is the value of $E\{\underline{e}(t)\underline{e}'(t)\}$ at $t = 0^-$, prior to the application of the initial disturbance $\underline{x}(0)$. $\underline{\Sigma}_o$ would be $\underline{0}$ if the system was initially at rest.

We wish to examine the effects of a specific initial condition $\underline{x}(0) = k\underline{\sigma}$, drawn from the distribution of $\underline{x}(0)$. Thus, the initial conditions for Eqs. (C-1)-(C-3) are

$$\underline{e}(0) = k\underline{\sigma}$$

$$\underline{x}(0) = k\underline{\sigma} \qquad \text{(C-6)}$$

$$\hat{\underline{x}}(0) = \underline{0}$$

and we seek expressions for the resultant system means and covariances.

System Error

Taking expectation of both sides of Eq. (C-3) gives

$$\dot{\bar{\underline{e}}}(t) = (\underline{A}-\underline{\Sigma}\ \underline{C}'\underline{V}^{-1}\underline{C})\bar{\underline{e}}(t) \qquad \bar{\underline{e}}(0) = k\underline{\sigma} \qquad \text{(C-7)}$$

Thus, the mean error is

$$\bar{\underline{e}}(t) = k\underline{\Phi}(t,0)\underline{\sigma} \qquad \text{(C-8)}$$

where $\underline{\Phi}$ is the transition matrix associated with $(\underline{A}-\underline{\Sigma}\ \underline{C}'\underline{V}^{-1}\underline{C})$,

$$\dot{\underline{\Phi}}(t,0) = (\underline{A}-\underline{\Sigma}\ \underline{C}'\underline{V}^{-1}\underline{C})\underline{\Phi}(t,0) \quad ; \quad \underline{\Phi}(0,0) = \underline{I} \qquad \text{(C-9)}$$

Subtracting Eqs. (C-7) and (C-3) next gives

$$\frac{d}{dt}(\underline{e}-\bar{\underline{e}}) = (\underline{A}-\underline{\Sigma}\ \underline{C}'\underline{V}^{-1}\underline{C})(\underline{e}-\bar{\underline{e}}) - \underline{\Sigma}\ \underline{C}'\underline{V}^{-1}\underline{v}(t) + \underline{w}(t)$$

$$E\{(\underline{e}-\bar{\underline{e}})(\underline{e}-\bar{\underline{e}})'\}|_{t=0} = \underline{\Sigma}_o$$

Therefore,

$$E\{[\underline{e}(t)-\bar{\underline{e}}(t)][\underline{e}(t)-\bar{\underline{e}}(t)]'\} = \underline{\Phi}(t,0)\underline{\Sigma}_o\underline{\Phi}'(t,0) + \int_0^t \underline{\Phi}(t,\tau)(\underline{\Sigma}\ \underline{C}'\underline{V}^{-1}\underline{C}\ \underline{\Sigma} + \underline{W})\underline{\Phi}(t,\tau)d\tau$$

which can be shown to be

$$\mathrm{cov}[\underline{e}(t)] = \underline{\Sigma}(t) - \underline{\Phi}(t,0)\underline{\sigma}\ \underline{\sigma}'\underline{\Phi}'(t,0) \qquad \text{(C-10)}$$

and which is independent of k.

State Estimate

We turn next to the estimate equation (C-2) to derive expressions for the mean and covariance of $\hat{\underline{x}}(t)$. The mean $\bar{\hat{\underline{x}}}$ is obtained by taking expectations, thus

$$\frac{d}{dt}\bar{\hat{\underline{x}}}(t) = \underline{\bar{A}}\ \bar{\hat{\underline{x}}} + \underline{\Sigma}\ \underline{C}'\underline{V}^{-1}\underline{C}\ \bar{\underline{e}}(t) \qquad \text{(C-11)}$$

since $\hat{\underline{x}}(0) = \underline{0}$ we have

$$\bar{\hat{\underline{x}}}(t) = k\cdot\int_0^t e^{\underline{\bar{A}}(t-\tau)}\underline{\Sigma}\ \underline{C}'\underline{V}^{-1}\underline{C}\ \underline{\Phi}(\tau,0)\underline{\sigma}d\tau \qquad \text{(C-12)}$$

$$\triangleq k\cdot\underline{\gamma}$$

To find the covariance of $\hat{\underline{x}}$ we define, for convenience, $\underline{\rho}(t) = \hat{\underline{x}}(t) - \underline{x}(t)$. Subtracting Eq. (C-11) from (C-2) gives for $\underline{\rho}(t)$,

$$\dot{\underline{\rho}}(t) = \overline{\underline{A}}\,\underline{\rho}(t) + \underline{\Sigma}\,\underline{C}'\underline{V}^{-1}[\underline{C}(\underline{e}-\overline{\underline{e}}) + \underline{v}(t)] \tag{C-13}$$

It is possible to also show that the bracketed term has the property

$$E\{[\underline{C}(\underline{e}-\overline{\underline{e}}) + \underline{v}(t)][\underline{C}(\underline{e}-\overline{\underline{e}}) + \underline{v}(\tau)]'\} = \underline{V}\delta(t-\tau) - \underline{C}\,\underline{\Phi}(t,0)\underline{\sigma}\,\underline{\sigma}'\underline{\Phi}'(\tau,0)\underline{C}' \tag{C-14}$$

Thus, using Eq. (C-13) we can show that

$$E\{\underline{\rho}(t)\underline{\rho}'(t)\} = \mathrm{cov}[\hat{\underline{x}}(t)] = e^{\overline{\underline{A}}t}\hat{\underline{X}}_o e^{\overline{\underline{A}}'t} + \int_0^t e^{\overline{\underline{A}}(t-\tau)}\underline{\Sigma}\,\underline{C}'\underline{V}^{-1}\underline{C}\,\underline{\Sigma}e^{\overline{\underline{A}}'(t-\tau)}d\tau - \underline{Y}\,\underline{Y}' \tag{C-15}$$

where $\hat{\underline{X}}_o$ is the variance of $\hat{\underline{x}}$ prior to t = 0.

System State

The mean of $\underline{x}(t)$ is simply the sum of Eqs. (C-8) and (C-12),

$$\overline{\underline{x}}(t) = k[\underline{\Phi}(t,0) + \int_0^t e^{\overline{\underline{A}}(t-\tau)}\underline{\Sigma}\,\underline{C}'\underline{V}^{-1}\underline{C}\,\underline{\Phi}(\tau,0)d\tau]\underline{\sigma} \tag{C-16}$$

Alternatively, from Eq. (C-1) $\overline{\underline{x}}(t)$ is also given by

$$\bar{\underline{x}}(t) = k[e^{\bar{\underline{A}}t} + \int_0^t e^{\bar{\underline{A}}(t-\tau)} \underline{B}\ \underline{L}\ \underline{\Phi}(\tau,0)d\tau]\underline{\sigma} \qquad \text{(C-16a)}$$

Lastly, to obtain an expression for the covariance of $\underline{x}(t)$, it is easiest to work from the relation

$$\text{cov}[\underline{x}(t)] = \text{cov}[\hat{\underline{x}}(t)] + \text{cov}[e(t)] - \underline{M}(t) - \underline{M}'(t)$$

where

$$\underline{M}(t) = E\{\hat{\underline{x}}(t)\underline{e}'(t)\} - \bar{\hat{\underline{x}}}(t)\bar{\underline{e}}'(t)$$

Expressions for the first two terms have already been derived. $\underline{M}(t)$ can be found by transposing and premultiplying Eq. (C-3) by $\hat{\underline{x}}(t)$ and postmultiplying Eq. (C-2) by $\underline{e}'(t)$. Summing and taking expectations gives[†]

$$\frac{d}{dt} E\{\hat{\underline{x}}(t)\underline{e}'(t)\} = \bar{\underline{A}}E\{\hat{\underline{x}}(t)\underline{e}'(t)\} + E\{\hat{\underline{x}}(t)\underline{e}'(t)\}'(\underline{A}-\underline{\Sigma}\ \underline{C}'\underline{V}^{-1}\underline{C})'$$
$$+ \hat{\underline{\Sigma}}\ \underline{C}'\underline{V}^{-1}\underline{C}(E\{\underline{e}\ \underline{e}'\}-\underline{\Sigma})$$

Thus, using Eqs. (C-8), (C-12) gives

$$E\{\hat{\underline{x}}(t)\underline{e}'(t)\} - \bar{\hat{\underline{x}}}(t)\bar{\underline{e}}'(t)$$

$$= -\int_0^t e^{\bar{\underline{A}}(t-\tau)}\underline{\Sigma}\underline{C}'\underline{V}^{-1}\underline{C}\ \underline{\Phi}(\tau,0)\underline{\sigma}\ \underline{\sigma}'\underline{\Phi}'(\tau,0)\cdot\underline{\Phi}'(t,\tau)d\tau$$

$$= -\underline{\Upsilon}\cdot\underline{\sigma}'\underline{\Phi}'(t,0) \qquad \text{(C-17)}$$

[†]Noting that $E\{\underline{v}(t)\underline{e}'(t)\} = -\frac{1}{2}\ \underline{C}\ \underline{\Sigma}(t)$, $E\{\hat{\underline{x}}(t)\underline{v}'(t)\} = \frac{1}{2}\ \underline{\Sigma}'\underline{C}$

Therefore

$$\text{cov}[\underline{x}(t)] = \underline{\Sigma}(t) + e^{\underline{\bar{A}}t}\hat{\underline{x}}_o e^{\underline{\bar{A}}'t} + \int_0^t e^{\underline{\bar{A}}(t-\tau)}\underline{\Sigma}\ \underline{C}'\underline{V}^{-1}\underline{C}\ \underline{\Sigma}e^{\underline{\bar{A}}'(t-\tau)}d\tau$$

$$- [\underline{\gamma}+\underline{\Phi}(t,0)\underline{\sigma}][\underline{\gamma}+\underline{\Phi}(t,0)\underline{\sigma}]' \qquad \text{(C-18)}$$

Modifications for Non-Zero Time Delay

When the time-delay τ is non-zero, the equations that govern optimal closed-loop behavior are

$$\dot{\underline{x}}(t) = \underline{A}\ \underline{x}(t) - \underline{B}\ \underline{L}\ \hat{\underline{x}}_2(t) + \underline{w}(t)$$

$$\dot{\hat{\underline{x}}}_2(t) = \underline{\bar{A}}\ \hat{\underline{x}}_2(t) + e^{\underline{A}\tau}\underline{\Sigma}(t-\tau)\underline{C}'\underline{V}^{-1}[\underline{C}\ \underline{e}_1(t-\tau) + \underline{v}(t-\tau)]$$

$$\dot{\underline{e}}_1(t-\tau) = (\underline{A}-\underline{\Sigma}\ \underline{C}'\underline{V}^{-1}\underline{C})\underline{e}_1(t-\tau) - \underline{\Sigma}\ \underline{C}'\underline{V}^{-1}\underline{v}(t-\tau) + \underline{w}(t-\tau)$$

$$\dot{\hat{\underline{x}}}_1(t-\tau) = \underline{A}\ \hat{\underline{x}}_1(t-\tau) - \underline{B}\ \underline{L}\ \hat{\underline{x}}_2(t-\tau) + \underline{\Sigma}\ \underline{C}'\underline{V}^{-1}[\underline{C}\underline{e}_1(t-\tau)+\underline{v}(t-\tau)]$$

where $\underline{e}_1(t-\tau) = \underline{x}(t-\tau) - \hat{\underline{x}}_1(t-\tau)$ is the estimation error at $t-\tau$ and $\hat{\underline{x}}_2$ is the best estimate of $\underline{x}(t)$ conditioned on $\hat{\underline{x}}_1(t-\tau)$. The total error is the estimation error plus prediction error $\underline{e}_2$. Thus

$$\underline{e}_1(t) + \underline{e}_2(t) = \underline{x}(t) - \hat{\underline{x}}_2(t) = \underline{e}(t)$$

Using the above equations and following the same procedures as in the earlier, no-delay, case, we can show for $t \geq \tau$

$$\text{cov}[\underline{e}(t)] = e^{\underline{A}\tau}\underline{\Sigma}(t-\tau)e^{\underline{A}'\tau} + \int_0^t e^{\underline{A}\xi}\underline{W}(t-\underline{\xi})e^{\underline{A}'\xi}d\xi$$

$$- e^{\underline{A}\tau}\underline{\Phi}(t-\tau,0)\underline{\sigma}\ \underline{\sigma}'\underline{\Phi}'(t-\tau,0)e^{\underline{A}'\tau}$$

(C-19)

$$\bar{\underline{e}}(t) = k \cdot e^{\underline{A}\tau}\underline{\Phi}(t-\tau,0)\underline{\sigma}^{\dagger} \tag{C-20}$$

$$\text{cov}[\hat{\underline{x}}_2(t)] = e^{\bar{\underline{A}}(t-\tau)}\hat{\underline{X}}_{\tau}e^{\bar{\underline{A}}'(t-\tau)} + \int_{\tau}^{t} e^{\bar{\underline{A}}(t-\xi)}e^{\underline{A}\tau}\underline{\Sigma}\ \underline{C}'\underline{V}^{-1}\underline{C}\ \underline{\Sigma}e^{\underline{A}'\tau}e^{\bar{\underline{A}}'(t-\xi)}d\xi$$

$$- \underline{\gamma}_2\underline{\gamma}_2' \tag{C-21}$$

$$\bar{\underline{x}}_2(t) = k\underline{\gamma}_2 \tag{C-22}$$

where

$$\underline{\gamma}_2 = \int_{\tau}^{t} e^{\bar{\underline{A}}(t-\xi)}e^{\underline{A}\tau}\underline{\Sigma}(\xi-\tau)\underline{C}'\underline{V}^{-1}\underline{C}\ \underline{\Phi}(\xi-\tau)d\xi \cdot \underline{\sigma}$$

and finally

$$\text{cov}[\underline{x}(t)] = e^{\underline{A}\tau}\underline{\Sigma}(t-\tau)e^{\underline{A}'\tau} + e^{\bar{\underline{A}}(t-\tau)}\hat{\underline{X}}_{\tau}e^{\bar{\underline{A}}'(t-\tau)} \tag{C-23}$$

$$+ \int_{\tau}^{t} e^{\bar{\underline{A}}(t-\xi)}e^{\underline{A}\tau}\underline{\Sigma}\ \underline{C}'\underline{V}^{-1}\underline{C}\underline{\Sigma}e^{\underline{A}'\tau}e^{\bar{\underline{A}}(t-\xi)}d\xi$$

$$- [\underline{\gamma}_2 + e^{\underline{A}\tau}\underline{\Phi}(t-\tau,0)\underline{\sigma}][\underline{\gamma}_2 + e^{\underline{A}\tau}\underline{\Phi}(t-\tau,0)\underline{\sigma}]'$$

$$\bar{\underline{x}}(t) = k[\underline{\gamma}_2 + e^{\underline{A}\tau}\underline{\Phi}(t-\tau,0)\underline{\sigma}] \tag{C-24}$$

or

$$\bar{\underline{x}}(t) = k[e^{\bar{\underline{A}}(t-\tau)}e^{\underline{A}\tau} + \int_{\tau}^{t} e^{\bar{\underline{A}}(t-\xi)}\underline{B}\ \underline{L}e^{\underline{A}\tau}\underline{\Phi}(\xi-\tau,0)d\xi]\underline{\sigma} \tag{C-24a}$$

---

†Note $\bar{\underline{e}}_1(t) = e^{\bar{\underline{A}}\tau}\bar{\underline{e}}(t-\tau)$

APPENDIX D

SYSTEM MODIFICATIONS FOR THRESHOLD CONSTRAINTS

In this appendix we derive a representation for threshold constraints that may be placed on displayed output variables. These constraints may arise from visual thresholds, i.e., a signal must move a fixed distance before motion is perceived by the human, or may arise from indifference thresholds, i.e., a human may not respond to a signal when it is sufficiently close to its nominal position.† In our analysis we do not distinguish between these effects.

We postulate that if $y(t) = \underline{c}'\underline{x}(t)$ is displayed, the human perceives the scalar signal

$$y_p(t) = f(y(t)) + v_y(t) \tag{D-1}$$

where $v_y(t)$ is the observation noise associated with $y(t)$ and $f(y)$ represents the nonlinear threshold element, viz

$$f(y) = \begin{cases} y-a & y \geq a \\ 0 & -a < y < a \\ y+a & y \leq -a \end{cases} \tag{D-2}$$

This element is shown in Fig. D1.

The signal $y(t)$ is assumed to be a Gaussian random variable with mean m and standard deviation σ, both of which may depend on t. The probability density of $y(t)$ is therefore

†Such thresholds have been considered before in the classical manual control literature [13]. However, they are usually ignored because of their relative unimportance in compensatory tracking tasks with "good" displays and relatively large signal variances.

$$p(y) = \frac{1}{\sqrt{2\pi}\,\sigma} e^{-(y-m)^2/2\sigma^2} \qquad \text{(D-3)}$$

Statistical Linearization

In our linearized analysis of the man-machine interface, we cannot include a nonlinearity of the form (Eq.D-2) directly, but must replace it by an equivalent gain $\hat{f}(y)$, as is common practice [14]. Since y(t) is assumed Gaussian, the Random-Input-Describing Function (RIDF) or statistical linearization finds pertinent application [14-15]. The RIDF is the linearized representation that minimizes the difference

$$d(t) = f(y(t)) - \hat{f}(y) \cdot y(t)$$

in a mean-squared statistical sense. Thus,

$$\hat{f}(y) = \arg\min E\{d^2\} \qquad \text{(D-4)}$$

It can be shown that

$$\hat{f}(y) = \int_{-\infty}^{\infty} y\, f(y)p(y)dy \left[\int_{-\infty}^{\infty} y^2 p(y)dy\right]^{-1} \qquad \text{(D-5)}$$

The RIDF may now be computed for the threshold (Eq.D-2). Substituting into Eq.(D-5) gives

$$(\sigma^2+m^2)\cdot\hat{f}(y) = \int_{-\infty}^{-a} (y^2+ay)e^{-(y-m)^2/2\sigma^2} \frac{dy}{\sigma\sqrt{2\pi}} + \int_{a}^{\infty} (y^2-ay)e^{-(y-m)^2/2\sigma^2} \frac{dy}{\sigma\sqrt{2\pi}}$$

Substituting $w = (y-m)/\sigma\sqrt{2}$, $\hat{a} = (a+m)/\sigma\sqrt{2}$ yields

$$\hat{f}(y) = [\gamma(m) + \gamma(-m)] \cdot (\sigma^2+m^2)^{-1}$$

where

$$\gamma(m) = \frac{1}{\sqrt{\pi}} \int_{-\infty}^{-\hat{a}} (2\sigma^2 w^2 + 2\sqrt{2}\, m\sigma w + m^2 + a\sigma w\sqrt{2} + am) e^{-w^2} dw$$

$$= \frac{2\sigma^2}{\sqrt{\pi}} \int_{-\infty}^{-\hat{a}} w^2 e^{-w^2} dw + \frac{(2m+a)\sigma\sqrt{2}}{\sqrt{\pi}} \int_{-\infty}^{-\hat{a}} w e^{-w^2} dw$$

$$+ \frac{(m^2+am)}{\sqrt{\pi}} \int_{-\infty}^{-\hat{a}} e^{-w^2} dw$$

Making use of the relations

$$\int_{-\infty}^{-b} w e^{-w^2} dw = -\frac{1}{2} e^{-b^2}$$

$$\int_{-\infty}^{-b} w^2 e^{-w^2} dw = \frac{1}{2}\left[\int_{-\infty}^{-b} e^{-w^2} dw - b e^{-b^2}\right]$$

gives

$$\gamma(m) = \frac{(\sigma^2+m^2+am)}{\sqrt{\pi}} \int_{-\infty}^{-\hat{a}} e^{-w^2} dw - \frac{\sigma m}{\sqrt{2\pi}} e^{-\hat{a}^2}$$

But,

$$\frac{2}{\sqrt{\pi}} \int_{-\infty}^{-b} e^{-w^2} dw = 1-\text{erf}(b) = \text{erfc}(b)$$

So that we finally obtain

$$\hat{f}(y) = \frac{1}{2}\left[(\sigma^2+m^2+am)\cdot\text{erfc}\left(\frac{a+m}{\sigma\sqrt{2}}\right) - \sigma m\sqrt{\frac{2}{\pi}}\, e^{-\left(\frac{a+m}{\sigma\sqrt{2}}\right)^2}\right.$$

$$\left. + (\sigma^2+m^2-am)\cdot\text{erfc}\left(\frac{a-m}{\sigma\sqrt{2}}\right) + \sigma m\sqrt{\frac{2}{\pi}}\, e^{-\left(\frac{a-m}{\sigma\sqrt{2}}\right)^2}\right]\cdot(\sigma^2+m^2)^{-1} \qquad \text{(D-6)}$$

as the linearized representation of the threshold element.

When y(t) is a zero-mean process, the above expression simplifies considerably to

$$\hat{f}(y) = \text{erfc}\left(\frac{a}{\sigma\sqrt{2}}\right) \qquad \text{(D-7)}$$

Thus, in our subsequent analysis it is assumed that the human perceives

$$y_p(t) \doteq \hat{f}(y)y(t) + v_y(t)$$

$$= \hat{\underline{c}}'\underline{x}(t) + v_y(t) \; ; \quad \hat{\underline{c}} = \hat{f}\,\underline{c} \qquad \text{(D-8)}$$

Furthermore, since only the quantity $\hat{\underline{c}}' V_y^{-1} \hat{\underline{c}}$ appears in the mathematical analysis, where V_y is the power density of the white observation noise v(t), it is possible to assume that the human perceives

$$y_p'(t) = y(t) + v_y(t)\hat{f}^{-1}(y) \quad . \tag{D-9}$$

The representations (Eq.D-8) and (Eq.D-9) are mathematically equivalent. Equation (D-9) is simpler to work with, however.

Foveal Viewing Conditions (m=0)

Under foveal viewing conditions, it has been found that the observation noise covariance V_y scales with the variance of y, viz

$$V_y = \rho_y \cdot \sigma_y^2 \tag{D-10}$$

where ρ_y is the "observation noise ratio" [6]. With the incorporation of threshold constraints one now associates with y(t) the noise $v_y'(t) = v_y(t) \cdot \hat{f}^{-1}(y)$ as in Eq.(D-9). Thus, the observation noise covariance V_y' is given by

$$V_y' = \rho_y \sigma_y^2 \cdot \hat{f}^{-2}(y)$$

$$= \rho_y \hat{\sigma}_y^2$$

where

$$\hat{\sigma} = \sigma \left[\operatorname{erfc}\left(\frac{a}{\sigma\sqrt{2}} \right) \right]^{-1} = \text{"equivalent" rms} \tag{D-11}$$

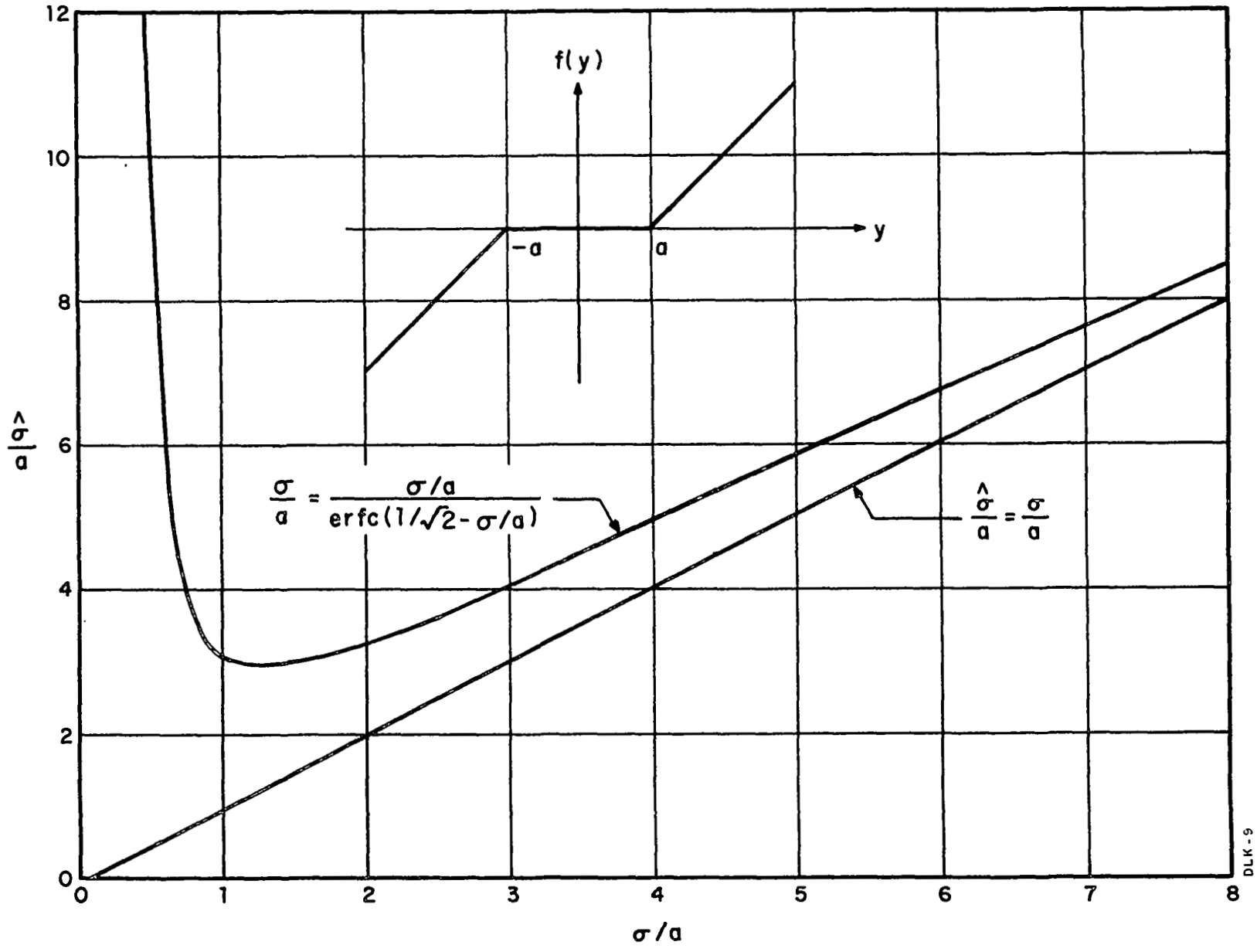

FIG. D-1 EQUIVALENT RMS AS A FUNCTION OF ACTUAL RMS FOR THRESHOLD NONLINEARITY

Thus, the observation noise associated with y(t) scales with $\hat{\sigma}$ and not with σ. Figure D1 shows $\hat{\sigma}/a$ as a function of σ/a. For $\sigma >> a$ we find $\sigma \sim \hat{\sigma}$ as expected. For $\sigma < a, \hat{\sigma}$ is very large since no useful information can be obtained from y(t) in this region.

It is interesting to compare the above results with those of Levison [16]. Levison assumes a model for $\hat{\sigma}_y^2$ of the form

$$\hat{\sigma}_y^2 = \sigma^2 + \sigma_e^2$$

which is linear in σ^2. If one fits a line to the linear part of $\hat{\sigma}/a$ in Fig. D1, the line would intersect the $\hat{\sigma}$ axis at about $\hat{\sigma} = 1.5a$. Thus,

$$\sigma_e^2 \sim 2.3\ a^2$$

A typical value for the visual (or indifference) threshold on position quantities is a = .05 degrees (3 min) of visual arc. Hence

$$\sigma_e^2 \sim 5.8 \times 10^{-3}\ \text{deg}^2$$

which agrees very well with the value of $\sigma_e^2 = 5.1 \times 10^{-3} \text{deg}^2$ as found by Levison.

Furthermore for $\sigma < a$, $\hat{\sigma}$ is very sensitive to small changes in σ. This is reflected in experimental results which showed high variability in data taken in "small signal" tracking tasks.[16]

Strategy Variations

There is an additional aspect of system behavior that can arise from threshold effects. Let us assume that the nominal cost functional to be minimized is

$$J(u) = E\left\{q_1^2 y^2 + g\,\dot{u}^2\right\} \tag{D-12}$$

and that y is a displayed variable. Since y is actually displayed, it is reasonable to expect that y in the cost functional (D-12) should in fact be the perceived y, namely y_p. Thus, one would argue that the human is attempting to minimize

$$J'(u) = E\left\{q_1^2 y_p^2 + g\,\dot{u}^2\right\}$$

$$= q_1^2 \sigma_{y_p}^2 + g\,\sigma_{\dot{u}^2}^2$$

$$= \left[q_1\ \mathrm{erfc}\left(\frac{a}{\sigma_y\sqrt{2}}\right)\right]^2 \sigma_y^2 + g\,\sigma_{\dot{u}}^2 \tag{D-13}$$

Consequently, for small signals one might expect control strategies that differ somewhat from those obtained when signal rms is much greater than threshold.† For smaller σ_y relatively more importance is placed on $\sigma_{\dot{u}}^2$ as the effective weighting on σ_y^2 decreases (for fixed g).

†Note that as $\sigma_y >> a$, erfc≈1.

Results of this nature have been found in experiment. Levison [16] conducted a series of identical k/s tracking tasks, but each having different display gains. As the display gain was decreased, the human controller gain was also found to decrease. When threshold effects are neglected, theory fails to predict this trend. However, further research is needed in this area to understand the inter-relation between display gain and controller strategy.